2-Hydroxypropyl-β-cyclodextrin is the active component in a triple combination formulation for treatment of Niemann-Pick C1 disease

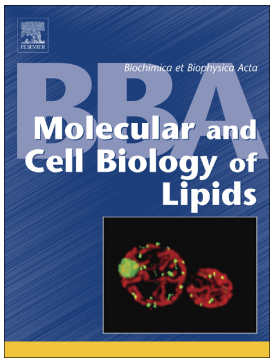

Jessica Davidson, Elizabeth Molitor, Samantha Moores, Sarah E. Gale, Kanagaraj Subramanian, Xuntian Jiang, Rohini Sidhu, Pamela Kell, Jesse Zhang, Hideji Fujiwara, Cristin Davidson, Paul Helquist, Bruce J. Melancon, Michael Grigalunas, Gang Liu, Farbod Salahi, Olaf Wiest, Xin Xu, Forbes D. Porter, Nina H. Pipalia, Dana L. Cruz, Edward B. Holson, Jean E. Schaffer, Steven U. Walkley, Frederick R. Maxfield, Daniel S. Ory

PII: S1388-1981(19)30064-2
DOI: https://doi.org/10.1016/j.bbalip.2019.04.011
Reference: BBAMCB 58451

To appear in: *BBA - Molecular and Cell Biology of Lipids*

Received date: 3 January 2019
Revised date: 25 April 2019
Accepted date: 26 April 2019

Please cite this article as: J. Davidson, E. Molitor, S. Moores, et al., 2-Hydroxypropyl-β-cyclodextrin is the active component in a triple combination formulation for treatment of Niemann-Pick C1 disease, BBA - Molecular and Cell Biology of Lipids, https://doi.org/10.1016/j.bbalip.2019.04.011

2-hydroxypropyl-β-cyclodextrin is the active component in a triple combination formulation for treatment of Niemann-Pick C1 Disease

Authors: Jessica Davidson[1], Elizabeth Molitor[1], Samantha Moores[1], Sarah E. Gale[1], Kanagaraj Subramanian[1], Xuntian Jiang[1], Rohini Sidhu[1], Pamela Kell[1], Jesse Zhang[1], Hideji Fujiwara[1], Cristin Davidson[2], Paul Helquist[3], Bruce J. Melancon[3], Michael Grigalunas,[3] Gang Liu,[3] Farbod Salahi,[3] Olaf Wiest[3], Xin Xu[4], Forbes D. Porter[5], Nina H. Pipalia[6], Dana L. Cruz[6], Edward B. Holson[7], Jean E. Schaffer[1], Steven U. Walkley[2], Frederick R. Maxfield[6], Daniel S. Ory[1*]

Affiliations:

[1]Department of Medicine, Washington University School of Medicine, St. Louis, MO 63110, USA

[2]Dominick P. Purpura Department of Neuroscience, Rose F. Kennedy Intellectual and Developmental Disabilities Research Center, Albert Einstein College of Medicine, 1410 Pelham Parkway South, Bronx, NY 10461, USA

[3]Department of Chemistry and Biochemistry, University of Notre Dame, Notre Dame, IN 46556 5670, USA

[4]Division of Preclinical Innovation, National Center for Advancing Translational Sciences (NCATS), 9800 Medical Center Dr., National Institutes of Health, Rockville, MD 20850, USA

[5]Section on Molecular Dysmorphology, *Eunice Kennedy Shriver* National Institute of Child Health and Human Development, NIH, DHHS, Bethesda, MD 20892, USA

[6]Department of Biochemistry, Weill Cornell Medical College, New York, NY 10065, USA

[7]KDac Therapeutics, Cambridge, MA 02139, USA

[*] To whom correspondence should be addressed: dory@wustl.edu

One Sentence Summary: HDACi are ineffective in treating NPC1 disease

ABSTRACT

Niemann-Pick type C1 (NPC1) disease is a fatal neurovisceral disease for which there are no FDA approved treatments, though cyclodextrin (HPβCD) slows disease progression in preclinical models and in an early phase clinical trial. Our goal was to evaluate the mechanism of action of a previously described combination-therapy, Triple Combination Formulation (TCF) – comprised of the histone deacetylase inhibitor (HDACi) vorinostat/HPβCD/PEG – shown to prolong survival in *Npc1* mice. In these studies, TCF's benefit was attributed to enhanced vorinostat pharmacokinetics (PK). Here, we show that TCF reduced lipid storage, extended lifespan, and preserved neurological function in *Npc1* mice. Unexpectedly, substitution of an inactive analog for vorinostat in TCF revealed similar efficacy. We demonstrate that the efficacy of TCF was attributable to enhanced HPβCD PK and independent of NPC1 protein expression. We conclude that although HDACi effectively reduce cholesterol storage in NPC1-deficient cells, HDACi are ineffective *in vivo* in *Npc1* mice.

1. INTRODUCTION

Niemann-Pick Type C (NPC) is a rare, autosomal recessive disease characterized by a defect in cholesterol trafficking with subsequent lysosomal lipid accumulation. The clinical presentation of NPC disease is variable. Age of onset ranges from perinatal to adulthood and initial manifestations may be visceral, neurologic, or psychiatric. Patients who survive past the perinatal stage will develop a progressive neurological disease that consists of cerebellar ataxia, dysarthria, dysphagia, and dementia, and ultimately leads to premature death [1]. NPC disease is caused by mutations in the NPC1 and NPC2 genes. NPC1 is a large transmembrane glycoprotein and NPC2 is a small, soluble protein; both proteins reside in lysosomes and facilitate cholesterol transport from that compartment [2-5]. Defects in the NPC1 gene are responsible for 95% of the disease, with over 400 mutations having been identified (https://medgen.medizin.uni-tuebingen.de/NPC-db2/index.php). The most prevalent NPC1 mutation, *NPC1*^{I1061T}, represents approximately 15-20% of all disease alleles [6, 7]. Previous studies have shown that the NPC1^{I1061T} protein is misfolded and targeted to endoplasmic reticulum (ER)-associated degradation (ERAD) through the proteasome [8]. The use of chemical chaperones or protein overexpression has been shown to partially correct the NPC1^{I1061T} phenotype by allowing a portion of the mutant protein to evade ERAD. NPC1^{I1061T} protein that escapes this checkpoint is then targeted to lysosomes where it is functional with respect to cholesterol trafficking [8].

There are currently no FDA approved treatments for NPC disease. Miglustat, an inhibitor of glycosphingolipid synthesis that has shown limited efficacy in treatment of NPC disease, is approved in over 40 countries, though not in the US [9]. The most promising therapeutic under evaluation is 2-hydroxypropyl-β-cyclodextrin (HPβCD), a cholesterol-binding compound. In preclinical models, treatment with HPβCD causes a reduction in unesterified cholesterol and glycolipid storage, prolonged survival, and a delay in clinical onset [10-12]. In a Phase 1/2a trial HPβCD was effective in slowing neurodegenerative disease progression in NPC1 patients and is currently being evaluated in a late stage clinical trial [13]. Because cyclodextrin is largely excluded by the blood brain barrier, optimal treatment requires direct central nervous system (CNS) delivery [11, 14-16].

A potentially more tractable therapeutic approach is the use of CNS-penetrant, small molecule proteostatic regulators, such as histone deacetylase (HDAC) inhibitors [17]. Through posttranslational modification of histones, transcription factors, and chaperones, HDACs can modify gene transcription and expression. HDAC inhibitors (HDACi) have been evaluated in a broad range of neurodegenerative disorders such as Alzheimer, Parkinson, and Huntington disease [18]. In previous studies, HDACi, including suberoylanilide hydroxamic acid (also known as vorinostat or SAHA), were found to be effective in reducing cholesterol storage in murine embryonic fibroblasts and human fibroblasts expressing the NPC1^{I1061T} protein [19-22]. While the mechanism of the correction is not well understood, treatment with the HDACi increased NPC1^{I1061T} expression through stabilization of the mutant protein, presumably through alteration of the proteostatic environment [21]. Intriguingly, when treated with HDACi, ~85% of all the NPC1 missense mutants tested exhibited reduced cholesterol storage, suggesting that proteostatic regulation may be relevant to large majority of NPC1 patients [21]. The potential proteostatic benefit of vorinostat is currently being evaluated in NPC1 patients in a Phase 1/2a trial [23].

Although HDACi appear to be effective *in vitro*, these findings have proved difficult to translate to *in vivo* models. Treatment of *Npc1*^{nmf164} mice, which harbor a D1005G point mutation, with 150mg/kg vorinostat in a PEG/DMSO vehicle led to normalization of expression of lipid homeostatic genes and limited improvement in liver pathology and function [24]. However, NPC1 mutant protein expression and lipid accumulation remained unchanged [24]. Moreover, vorinostat did not show efficacy with respect to disease progression, life span, or weight loss, which is unsurprising in light of its poor blood brain barrier penetration [25]. In an effort to circumvent this limitation, Alam and colleagues proposed a triple combination formulation (TCF), in which both vorinostat and HPβCD were complexed in a PEG/DMSO vehicle [26, 27]. Treating *Npc1*^{nmf164} mice with the TCF led to an almost two-fold increase in lifespan relative to mice treated with HPβCD alone. They reported greater exposure of the plasma and brain to vorinostat with the TCF, attributing the benefit to improved drug pharmacokinetics (PK) [26, 27]. Although the formulation appears to offer an attractive approach to improving HDACi efficacy *in vivo*, the results are difficult to interpret due to the confounding use of HPβCD in the formulation.

In the present study, we evaluate the effects of the TCF formulation in the *Npc1*$^{I1061T/I1061T}$ mouse model, which express the prevalent I1061T point mutation, and in BALB/c *Npc1*^{nih} (*Npc1*$^{-/-}$) mice. Using additional controls, such as an inactive analog of vorinostat and HPβCD dissolved in the PEG/DMSO vehicle, we show that TCF efficacy results from enhanced HPβCD PK rather than enhanced HDACi activity. Our findings of lack of efficacy for the HDACi *in vivo* should prompt reevaluation of the application of these drugs for treatment of NPC1 and other diseases.

2. MATERIALS AND METHODS

2.1. Study Design

The study objectives were to evaluate the Triple Combination Formulation (TCF) [26] as a therapeutic for Niemann-Pick C and determine its mechanism of action in a murine model. For the 6-week treatment regimen and survival studies, *Npc1*$^{tm(I1061T)Dso}$ mice [22] were randomly allocated to one of ten different treatment groups: vehicle, HPβCD in vehicle (CD/Vehicle), HPβCD in water (CD/H_2O), HPβCD in water delivered 3x weekly (CD/H_2O (3x/wk)), vorinostat, the inactive analog of vorinostat (IVA), TCF with vorinostat (TCF Active), TCF with inactive vorinostat (TCF/IVA), and TCF with CI-994 (TCF/CI994). A parallel 6-week study was performed in BALB/c *Npc1*^{nih} mice to determine dependency on NPC1 mutant protein expression. This study included three of the treatment groups: vehicle, CD/H_2O, and TCF.

2.2. Animals

For treatment studies, *Npc1*$^{tm(I1061T)Dso}$ (*NPC1*^{I1061T}) and BALB/c *Npc1*^{nih} (*NPC1*$^{-/-}$) mice were used. NPC1^{I1061T} mice harbor the clinically relevant p.I1061T mutation in the *Npc1* gene [22]. *Npc1*$^{-/-}$ carries a null mutation gene due to a retroposon insertion in the *NPC1* locus [28, 29]. Breeding colonies of the NPC1 mouse lines are maintained at Washington University. C57BL/6J mice obtained from Jackson Laboratories (Bar Harbor, ME, USA) were used for PK analysis and as wild type controls. Mice were kept in a temperature and humidity-controlled animal facility and were given access to standard chow and water *ad libitum.* Experimental procedures were approved by the Washington University Animal Studies Committee and were conducted in accordance with the USDA Animal Welfare Act and the Public Health Service Policy for the Humane Care and Use of Laboratory Animals.

2.3. Materials

All chemicals including powdered 2-hydroxypropyl-β-cyclodextrin (H107), DMSO, polyethylene glycol (PEG400), methoxypolyethylene glycol 350 (MeO-PEG-350) ammonium fluoride and citric acid were purchased from Sigma-Aldrich (St. Louis, MO, USA). Vorinostat (suberanilohydroxamic acid), inactive vorinostat (suberanilic acid), d5-vorinostat, and d5-inactive vorinostat were synthesized in-house initially in the Helquist lab and later by the Notre Dame Chemical Synthesis Drug Discovery Facility following published procedures [30]. The LC-MS grade methanol, isopropanol, and acetonitrile were purchased from Honeywell (Morristown, NJ).

2.4. Synthesis of inactive vorinostat

Octane-1,8-dioic acid was purchased from Ark Pharma (Libertyville, IL). A solution of octane-1,8-dioic acid (5.00 g, 28.7 mmol) in acetic anhydride (10 mL) was heated at reflux for 1 h. The mixture was cooled to 25°C and concentrated under vacuum. The remaining yellow solid was recrystallized from acetonitrile to afford the cyclic anhydride (1.75 g; 20%) as a white solid, which was used in the next step. The anhydride was dissolved

in anhydrous THF (50 mL), and aniline (1.03 g, 1.01 mL; 11.1mmol) was added to the solution at 25 °C. After being stirred for 30 min, the mixture became cloudy white. Water (20 mL) was added, and the resulting white solid was isolated by filtration. Recrystallization from water gave 8-oxo-8-(phenylamino)octanoic acid (0.92 g, 33%) as a white powder. ^{1}H NMR (400 MHz, CH_3OD) δ 7.54 (d, 2H), 7.27 (t, 2H), 7.06 (m, 1H) 2.30 (m, 2H), 2.27 (m, 2H), 1.61 (m, 4H), 1.39 (m, 4H). ^{13}C NMR (126 MHz, CH_3OD) δ 176.43, 173.45, 138.72, 128.58, 120.08, 36.72, 33.67, 28.82, 28.75, 25.59, 24.75. HRMS *m/z* calculated for $C_{14}H_{20}NO_3$ (M+1) 250.1438; found 250.1457. (lit.[30] ^{1}H NMR, ^{13}C NMR).

2.5. Dose response of fibroblasts and bone marrow-derived macrophages

As previously described [21], human *NPC1^{I1061T}* fibroblasts were grown in Modified Eagle Medium (MEM) supplemented with 10% FBS. For drug treatment, cells were maintained in MEM supplemented with 5% FBS. These cells were seeded in 384-well plates at 450 cells/well in growth medium on day one. After overnight incubation, test compounds were added at 40 nM to 10 μM final concentration. DMSO was used as a control treatment in each plate. After 72 hours, the plate was washed with PBS three times, fixed with 1.5% PFA, and stained with 50 μg/ml filipin and the nuclear stain Draq5. Measurements were made from four wells for each condition in each experiment, and the experiment was repeated three times. Images were acquired on an ImageXpress^{Micro} automatic fluorescence microscope, at four sites per well and analyzed to obtain the LSO compartment ratio, which is a measure of filipin labeling of stored cholesterol [19, 20]. A high LSO ratio is associated with high levels of cholesterol in late endosomes/lysosomes. The LSO compartment ratio for each concentration was normalized to the DMSO treated controls. The identical procedure was used for bone marrow derived macrophages, which were obtained from the femurs of *Npc1$^{I1061T/I1061T}$* mice.

2.6. Drug preparations and regimen

Vorinostat formulations and TCF active were prepared as described [26]. The inactive formulations and TCF/CI994 were prepared in the same manner using the inactive analog of vorinostat and CI-994, respectively. HPβCD was dissolved in either the 45% PEG/5% DMSO vehicle or water, as specified. Final compositions of all formulations are summarized in **Table 1**, and were prepared fresh for each use and filtered prior to delivery. In HPβCD-containing formulations, final concentration was 2000 mg/kg, except in the CD/H_2O (3x/wk), in which the final concentration was 4000 mg/kg. Treatments began at four weeks of age and were administered weekly for the duration of the six-week study, with the exception of CD/H_2O (3x/wk), in which the treatment was delivered three times per week. Animal body weight was determined before each injection. All treatments were administered via intraperitoneal injection at a dose of 10 μL/g body weight. For survival studies, mice were euthanized when they showed clinical signs of end-stage disease as previously described [10].

2.7. Gait analysis

Gait analysis was performed using the Noldus CatWalk XT 10.6 (Noldus Information Technology, Wageningen, Netherlands). CatWalk XT is a highly sensitive tool to assess gait and locomotion. Gait analysis was performed

once per week, prior to compound injection. The following data were analyzed: standing on diagonal, coupling, and stride length. Standing on diagonal describes the relative duration of simultaneous contact with the glass plate of all combinations of paws. Coupling, a measure of inter-paw coordination, is the temporal relationship between the placement of a pair paws relative to the duration of a step cycle. Stride length is the distance between two successive placements of the same paw.

2.8. Tissue collection

Mice were euthanized according to established procedures one-hour post final treatment. Euthanasia was performed via ketamine/xylazine cocktail and mice were perfused with 0.9% saline. Plasma was collected via retroorbital bleed. Liver and brain tissue were resected with one lobe of liver, half of the cortex, and the whole cerebellum fixed in 4% paraformaldehyde for tissue histology. All remaining liver and the remaining half of the cortex were flash frozen in liquid nitrogen and stored at -80°C until use.

2.9. Pharmacokinetics

Five-week-old male C57BL/6J (000664) mice were purchased from Jackson Laboratories (Bar Harbor, ME, USA). Mice were enrolled into seven treatment groups with five harvest time points per group and n=4 mice per harvest time point. Across all treatment groups, a dose of 10 µL/g of body weight was used and all drug compounds were delivered via a single intraperitoneal injection. Tissue harvests occurred at 0.25, 1, 2, 4, or 7 hours post injection as indicated above.

For the quantification of vorinostat and IVA, each liquid chromatography-tandem mass spectrometry (LC-MS/MS) run included eight calibration standards in duplicate, one blank, one blank without IS, and study samples. The internal standards (IS) for plasma and liver (600/600/30,000 ng/mL d5-vorinostat/d5-suberanilic acid/HP-d6-β-CD) and for brain (100/100/5000 ng/mL d5-vorinostat/d5-suberanilic acid/HP-d6-β-CD) were prepared by dilution of d5-vorinostat, d5-suberanilic acid, and HP-d6-β-CD stock solutions with methanol-water (1:1). The PEG-400 IS spiking solutions for liver (2 µg/mL MeO-PEG-350) and for brain (1 µg/mL MeO-PEG-350) were prepared by dilution of MeO-PEG-350 stock solution with acetonitrile. Brain samples were homogenized in 4 volumes of Milli Q water and liver samples in 0.04 M of citric acid in water for analysis of vorinostat/suberanilic acid/HPβCD. For PEG400, brain and liver samples were homogenized in 4 volumes of Milli Q water.

LC-MS/MS analysis was conducted on a Shimadzu (Columbia, MD) Prominence UFLC system coupled with an Applied Biosystems/MDS Sciex (Ontario, Canada) 4000QTRAP mass spectrometer using positive multiple reaction monitoring (MRM). Separation of vorinostat and suberanilic acid was carried out using a Waters (Milford, MA) Xselect HSS C18 analytical column (3 × 50 mm, 3.5 µm) connected to a Phenomenex (Torrance, CA) SecurityGuard C18 guard column (4 × 3 mm) at a flow rate of 0.6 mL/min. The mobile phase consisted of 5 mM ammonium fluoride in water (solvent A), and 0.1% formic acid in methanol-acetonitrile (4:1) (solvent B). The step gradient was as follows: 0–0.1 min, 50% solvent B; 0.1–1.5 min, 50% to 100% solvent B; 1.5–2.0 min, 100% solvent B; 2.0–2.1 min, 100% to 50% solvent B; 2.1–3.5 min 50% solvent B. The HPLC

eluate was directed into the mass spectrometer for data acquisition within the 1.6-min time window (0.8 – 2.4 min) in which vorinostat and suberanilic acid were eluted; elsewhere, eluate was sent to waste to minimize source contamination. The total run-time was 3.5 min. The injection volume was 5, 10, 20 µL for plasma, liver, and brain samples, respectively. The ESI source temperature was 600 °C; the ESI needle was 2000 V; the declustering potential was 50 V; the entrance potential was 10 V; and the collision cell exit potential was 10 V for vorinostat, suberanilic acid, d5-vorinostat, and d5-suberanilic acid. The collision and curtain gas were set at medium and 20, respectively. Both desolvation gas and nebulizing gas were set at 55 L/min and 35 L/min, respectively. The collision energies were 17, 32, 17, and 32 eV for vorinostat, suberanilic acid, d5-vorinostat, and d5-suberanilic acid, respectively. MRM mass transitions *m/z* 265.2→172.1, 250.2→94.1, 270.2→172.1, and *m/z* 255.2→94.1 were used for vorinostat, suberanilic acid, d5-vorinostat, and d5-suberanilic acid, respectively, with a dwell time of 50 ms for each mass transition. The mass spectrometer was operated at unit mass resolution for both the first and third quadruple.

Sample preparation, instrumentation, LC-MS/MS conditions, and quantification of cyclodextrin by tandem mass spectrometry were performed as previously reported [31]. Data were acquired and analyzed by Analyst software (version 1.5.2).

For analysis of PEG400, the mobile phase consisted of 5 mM ammonium acetate in water (solvent A), methanol (solvent B), and isopropanol (solvent C). Separation of PEG-400 and MeO-PEG-350 was carried out using solvent A and B on a Waters (Milford, MA) Xbridge C18 analytical column (3 × 50 mm, 3.5 µm) connected to a Phenomenex (Torrance, CA) SecurityGuard C18 guard column (4 × 3 mm) at a flow rate of 0.6 mL/min. The step gradient for solvents A and B was as follows: 0 – 3.0 min, 20% to 50% solvent B; 3.0–3.1 min, 50% to 20% solvent B; 3.1–6.5 min 20% solvent B. The solvent A and B eluate was controlled by valve 1 and directed into the mass spectrometer for data acquisition within the 1.6-min time window (1.2 – 3.0 min) in which PEG-400 and MeO-PEG-350 were eluted; elsewhere, eluate was sent to waste to minimize source contamination. Solvent C is controlled with valve 2 and used to back flush column after PEG-400 and MeO-PEG-350 were eluted at 0.6 mL/min for 1.5 min (3.0 – 4.5 min). The total run-time was 6.5 min. The injection volume was 5 µL for liver and brain samples. The ESI source temperature was 650°C; the ESI needle was 5000 V; the declustering potentials was 35 and 80 V for PEG-400 and MeO-PEG-350, respectively; the entrance potential was 10 V for both PEG-400 and MeO-PEG-350; and the collision cell exit potential was 10 V for both PEG-400 and MeO-PEG-350. The collision and curtain gas were set at medium and 20, respectively. Both desolvation gas and nebulizing gas were set at 65 L/min and 55 L/min, respectively. The collision energies were 30 eV for both PEG-400 and MeO-PEG-350. The multiple reaction monitoring (MRM) mass transitions *m/z* 344.1→133.1, and *m/z* 314.1→103.1 were used for PEG-400 and MeO-PEG-350, respectively, with a dwell time of 50 ms for each mass transition. The mass spectrometer was operated at unit mass resolution for both the first and third quadruple.

Pharmacokinetic parameters were calculated with the mean concentrations of 3-4 mice at each time point using the non-compartmental method (NCA; Model 200) of the pharmacokinetic software Phoenix

WinNonlin (Certara, St. Louis, MO). The area under the concentration-time curve (AUC) was calculated using the linear trapezoidal method.

2.10. Measurement of histone acetylation

Tissues were homogenized and sonicated in TNEN buffer (1% NP-40, 0.25mM EDTA, 50mM Tris pH 8, 150mM sodium chloride) with 1x protease complete inhibitors and 1mM phenylmethylsulfonyl fluoride. The lysate was centrifuged for 10 min at 10,000 × *g* at 4°C. Supernatant was collected and protein quantified using a BCA Protein Assay kit (Pierce). Equal amounts of protein were loaded and separated by NuPage 4-12% Bis-Tris gel (Invitrogen) under reducing conditions with 1x MES running buffer (Invitrogen). Proteins were transferred to nitrocellulose using the iBlot 2 dry transfer system (Invitrogen) and probed with rabbit anti-human histone H3 polyclonal antibody at a 1:10,000 dilution (Abcam) and rabbit anti-human acetyl-histone H3 polyclonal antibody at a 1:1000 dilution (Millipore). A rabbit anti-human Hsp90 (Enzo) was used as a protein loading control. Peroxidase-conjugated donkey anti-rabbit IgG (Jackson ImmunoResearch Laboratories) and chemiluminescence were used for detection.

2.11. Measurement of NPC1 protein expression

For quantification of NPC1 protein expression in liver, tissues were homogenized and sonicated in HEPES buffer (50mM Tris pH 8, 150mM sodium chloride, 5mM EDTA, 1% Triton X-100, 0.1%SDS) with 1x protease complete inhibitors and 1mM phenylmethylsulfonyl fluoride. The lysate was centrifuged for 10 min at 10,000 × *g* at 4°C. Supernatant was collected and protein quantified using a BCA Protein Assay kit (Pierce). Sample protein was incubated overnight at 4°C with 1.8µg of a rabbit polyclonal antibody raised against mouse NPC1 (amino acids 1261–1278, CTTYERYRGTERERLLNF) and produced in-house [32]. Immunoprecipitation was performed using Dynabeads Protein A (Thermo Fisher) and protein was eluted using 2x Laemmli sample buffer (Bio-Rad) with 5% 2-mercaptoethanol. Samples were separated by NuPage 3-8% Tris-Acetate gel (Invitrogen) under reducing conditions with 1x Tris-Acetate running buffer (Invitrogen). Proteins were transferred to nitrocellulose using the iBlot 2 dry transfer system (Invitrogen) and probed with aforementioned mouse-NPC1 antibody at a concentration of 1:1000. Protein detection was performed as described above.

For quantification of NPC1 protein expression in brain, membrane proteins in tissues were isolated using a membrane protein extraction kit, Mem-PER Plus (Thermo Scientific), and quantified using a BCA Protein Assay kit (Pierce). Samples were separated by NuPage 3-8% Tris-Acetate gel (Invitrogen) under reducing conditions with 1x Tris-Acetate running buffer (Invitrogen). Proteins were transferred to nitrocellulose using the iBlot 2 dry transfer system (Invitrogen). NPC1 expression was analyzed using the rabbit polyclonal antibody raised against human NPC1 C-terminus described above. Detection of p63 by a rabbit polyclonal antibody [33] was used as a loading control. Their respective concentrations were 1:1000 and 1:5000. Peroxidase-conjugated donkey anti-rabbit IgG (Jackson ImmunoResearch Laboratories) and chemiluminescence were used for detection.

2.12. Lipidomic analysis

The tissue samples were homogenized with 8-fold excess volume of PBS buffer using an Omni Bead Ruptor 24 (Omni International, Inc.). 50 µL of the tissue homogenate was extracted with 200 µL of methanol containing internal standards. For sterol analysis, d7-cholestane-3β,5α,6β-triol, d7-7-ketocholesterol, d7-24(S)-hydroxycholesterol, and d7-cholesterol were used as the internal standards. All sterols as well as their deuterated standards were derivatized with N, N-dimethylglycine. For sphingolipid measurements, 17:0 glycosylceramide, d3-16:0 lactosyl-ceramide, d7-sphingosine, d7-sphingosine-1-phosphate, N-omega-CD3-octadecanoyl monosialoganglioside GM3, and N-heptadecanoylceramide trihexoside were added as the internal standards. Lipid analysis was performed by LC-MS/MS as previously described [22, 34].

2.13. Histopathological analysis

Liver and brain tissue samples fixed in 4% paraformaldehyde and stored cold in 0.1 M phosphate buffer were sectioned at 35 microns on a Vibratome and subjected to filipin staining (liver and brain) and to GM2 immunohistochemical staining (brain only). Staining procedures followed published methods [10, 35]. Briefly, for filipin labeling, prepared sections were incubated with PBS containing 0.005% filipin complex (Sigma F9765) from a 25 mg/mL solubilized stock in DMSO (Sigma D128-500), or with an equivalent concentration of DMSO only to serve as a control. The sections were mounted on Gold Seal fluorescent antibody slides (Fisher 12-568-20) with Prolong Antifade Kit (Molecular Probes P7481) and circular coverslips (Fisher 12-545-81). For GM2 staining, prepared sections were incubated overnight at 4°C in diluent with primary antibody to GM2 ganglioside (produced in house) or with nonspecific mouse IgM (Sigma) as control. On day 2, the sections were incubated with the secondary antibody (Texas Red-conjugated goat anti-mouse IgM), and mounted as previously described for filipin labeling. Prepared slides were imaged on a Leica fluorescence microscope.

Blinded analysis by two independent reviewers was carried out on sections that were coded independently by a third party. A scale of 0 – 5 was used to evaluate staining intensity as an indicator of relative storage of cholesterol and GM2 ganglioside (0 = no storage, 5 = extensive storage present). In liver, cholesterol storage was assessed based on staining intensity and the distribution of filipin staining in hepatocytes and liver macrophages (Kupffer cells). The identity of the latter were established by evaluation of CD68 stained cells in liver sections which reveal the typical distribution of Kupffer cells vs. hepatocytes. In brain, assessments were carried on for both GM2 ganglioside and cholesterol, focusing on upper (layers 1-3) and lower (4-6) dorsal neocortex. Brain sections were matched so that analysis occurred just above the dorsal placement of the hippocampus at -1.6-2.0 from the bregma (based on Franklin and Paxinos, *The Mouse Brain in Stereotaxic Coordinates*, 3rd edition). Following completion of scoring, the third party code was broken and scoring results of all sections were averaged for each tissue area and statistical analyses performed using an ANOVA (significance deemed $p<0.05$). If warranted, Dunnett's test was employed to determine significant differences between vehicle and treatment groups.

2.14. HDAC inhibitor treatment of bone marrow-derived macrophages

Bone marrow was isolated from *Npc1*^{I1061T} mice that were housed in a pathogen-free environment at Albert Einstein College of Medicine and used in accordance with protocols approved by the Institutional Animal Care and Utilization Committees. Sterilized femurs and tibias from *Npc1*^{I1061T} mice were flushed in bone marrow (BM) media (DMEM with L-Glutamine, 4.5 g/L glucose, sodium pyruvate and 1% penicillin/streptomycin, supplemented with 10% heat-inactivated fetal calf serum (FCS) and 20% L-cell conditioned medium). Cells were differentiated for seven days by culturing in BM media in a humidified atmosphere (5% CO_2) at 37°C.

For vorinostat treatment and filipin staining, differentiated BMMs were plated in 384 well plates in BM media. On the following day vorinostat was added at concentrations from 0.004 µM to 10 µM in 4-6 wells per dose, and the cells were incubated in control medium or vorinostat for 48h or 72h. To load the BMMs with lipoprotein, the cells were supplemented for the final 24 hours with 20 µg/ml acetylated low density lipoprotein (AcLDL). At the end of the treatment cells were washed with phosphate buffered saline (PBS), fixed with 2% para-formaldehyde (PFA) in PBS and stained with filipin and Draq5. Automated microscopy and data analysis was performed as described in section 2.5.

3. RESULTS

3.1. Characterization of an inactive vorinostat control

We reasoned that if HPβCD was the active component in the TCF, then a formulation containing the PEG/DMSO vehicle, but lacking HDACi activity, would show similar efficacy in an NPC1 mouse model. We selected suberoylanilide acid, an inactive analog and synthetic precursor of suberoylanilide hydroxamic acid (vorinostat)[30] for inclusion in TCF (Fig. 1A) to minimize perturbation to the formulation. In contrast to vorinostat, which reduces lysosomal cholesterol in human fibroblasts with homozygous *NPC1*^{1061T} mutations (Fig. 1B), suberoylanilide acid (inactive vorinostat, IVA), had no effect on cholesterol storage. To demonstrate that IVA lacks HDACi activity *in vivo*, the inactive compound along with a vorinostat control were injected into mice – both alone and as a component of TCF – and liver acetylation of histone H3 was assessed one hour post injection, a method similarly used by Alam et al [26]. Levels of both acetylated and total histone 3 were determined by western blot, and their ratio used to determine acetylation status. Increased histone 3 acetylation was observed in treatment groups containing an active HDACi: vorinostat alone, TCF containing vorinostat (TCF active), and TCF containing CI-994 (TCF/CI-994) [36], a more CNS-penetrant HDACi (Fig. 1C). No increase in acetylation was observed in treatment groups not containing an active HDACi, including groups treated with IVA and TCF/IVA. Together, these findings support use of suberoylanilide acid as an inactive analog for examination of the TCF mechanism.

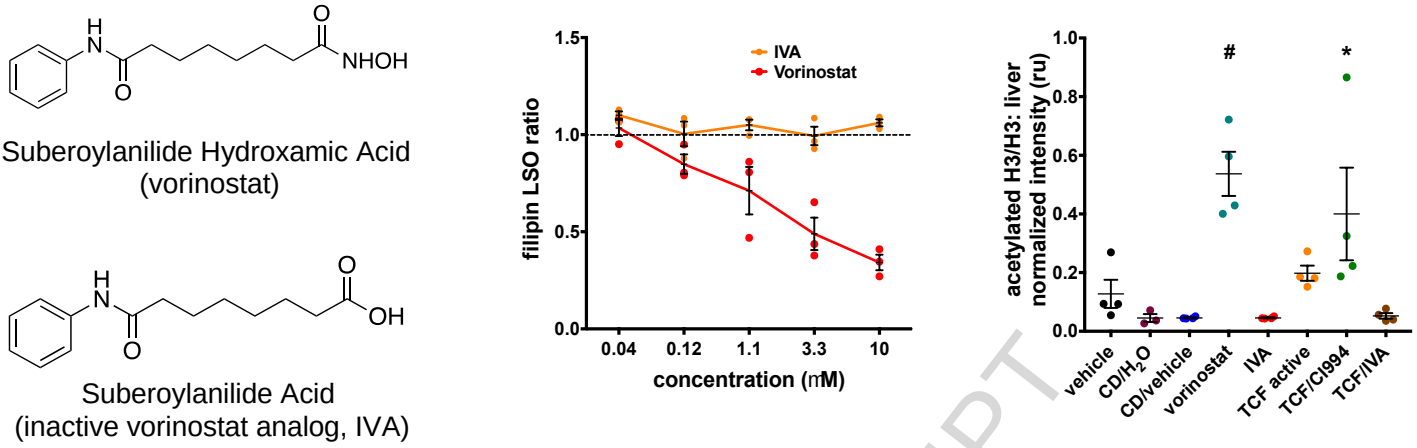

Figure 1. Inactive vorinostat control. (**A**) Structures of suberoylanilide hydroxamic acid (vorinostat) and suberoylanilide acid (inactive vorinostat, IVA). (**B**) Dose response of *NPC1*$^{I1061T/I1061T}$ fibroblasts to vorinostat and IVA. After 72h of treatment, cells were PFA fixed and stained with filipin to detect cholesterol. The total instensity of lysosomal storage organelle (LSO) filipin per cell area was determined using the LSO comparatment ratio (total intensity above a high threshold/number of pixels above low threshold). Data are shown as mean±SEM (n=3). (**C**) Assessment of acetyaltion status of histone H3 (H3) in mice by western blotting. Wild type C57BL/6J were given a single dose of the specified compound and harvested 1h post injection. Data are presented as mean ± SEM of the ratio of acetylated H3 to total H3, after normalization to an Hsp90 loading control. All groups are n=4 and statistical analysis was done versus vehicle control using an ANOVA with Dunnett's test to determine significance. *, $p<0.05$; #, $p<0.01$.

3.2. Pharmacokinetic analysis of TCF formulation components

In order to evaluate the potential interaction between the individual components of TCF (Table 1), we performed PK studies for vorinostat, HPβCD and the PEG400 vehicle. Mice were administered a single intraperitoneal dose of the specified treatment, and plasma, liver, and brain samples were harvested at 0.25, 1, 2, 4, and 7 hours after injection. Vorinostat, HPβCD and PEG400 concentrations were determined by LC-MS/MS. The C_{max} for vorinostat in plasma was not significantly different between vorinostat in vehicle and in TCF, though the area under the curve (AUC_{last}) for vorinostat in TCF was increased 31%. In the liver tissue, TCF increased vorinostat C_{max} and AUC_{last} by 18% and 27%, respectively (Table 2). Similarly, in the brain tissue, TCF increased vorinostat C_{max} and AUC_{last} by 55% and 50%, respectively. These findings suggest that in the presence of the PEG400 and HPβCD there is reduced clearance of the drug from plasma, resulting in increased tissue penetration. By contrast, PEG400 altered plasma HPβCD PK by lowering the C_{max} and increasing time to peak concentration (T_{max}). This was accompanied by a significant increase in AUC_{last} for HPβCD in all formulations containing PEG400 (CD/vehicle, TCF active and TCF/IVA), as compared to water vehicle (Table 3). Compared with CD/water, the liver tissue exposure (AUC_{last}) for the HPβCD-containing formulations was increased 36%, 37% and 25% in the CD/vehicle, TCF active and TCF/IVA groups, respectively, and the brain tissue exposure (AUC_{last}) for the HPβCD-containing formulations was increased

106%, 129% and 95% in the CD/vehicle, TCF active and TCF/IVA groups. There was no clear relationship between the PEG400 PK with respect to the presence or absence of HPβCD or the HDACi, although addition of either component increased C_{max} and AUC_{last} as compared to vehicle alone (Supplemental Table 1). Taken together, these findings demonstrate that inclusion of the PEG400 vehicle in the formulations increased tissue exposures for vorinostat and HPβCD by increasing plasma concentrations of the drugs.

	Treatment	H_2O	5% DMSO, 45% PEG	2000 mg/kg HPβCD	4000 mg/kg HPβCD	50 mg/kg vorinostat	30 mg/kg CI-994
NPC1-I1061T	vehicle		+				
	CD/vehicle		+	+			
	CD/H_2O	+		+			
	CD/H_2O (3x/wk)	+			+		
	vorinostat		+			active	
	IVA		+			inactive	
	TCF active		+	+		active	
	TCF/IVA		+	+		inactive	
	TCF/CI994		+	+			+
NPC1-/-	vehicle		+				
	CD/vehicle		+	+			
	TCF active		+	+		active	

Table 1. Composition of formulations. *NPC1*$^{I1061T/I1061T}$ mice and *Npc1*$^{-/-}$ were allocated to one of the following treatment groups and were treated weekly (with the exception of the CD 3x/wk group) over 6-weeks. The compositions of all formulations are listed below, and the same compositions were used for PK studies.

Vorinostat Pharmacokinetic Parameters				
			Treatment	
			vorinostat	TCF active
Matrix	Parameters	Unit		
Plasma	C_{max}	ng/mL	10495	10683
	T_{max}	hr	0.25	0.25
	AUC_{last}	ng•hr/mL	7535	9893
	AUC_{inf}	ng•hr/mL	7604	9897
	$t_{1/2}$	hr	0.68	0.326
Liver	C_{max}	ng/mL	209	247
	T_{max}	hr	0.25	0.25
	AUC_{last}	ng•hr/mL	513	650

Brain	C_{max}	ng/mL	1163	1800
	T_{max}	hr	0.25	0.25
	AUC_{last}	ng•hr/mL	1238	1857

Table 2. Pharmacokinetics for vorinostat in plasma, liver, and brain tissues. C57BL/6J wild type mice were administered a single dose of vorinostat or TCF active and harvested 0.25, 1, 2, 4, or 7 hours post-injection. Vorinostat drug levels were measured via LC-MS/MS. PK values were calculated from the average of n=4 mice per time point, and are shown for plasma, liver, and brain samples.

Cyclodextrin Pharmacokinetic Parameters						
			Treatment			
			CD/vehicle	CD/H_2O	TCF active	TCF/IVA
Matrix	Parameters	Unit				
Plasma	C_{max}	µg/mL	3880	5375	4718	3477
	T_{max}	hr	1	0.25	1	1
	AUC_{last}	µg•hr/mL	6730	4556	9883	6100
	AUC_{inf}	µg•hr/mL	6731	4558	9887	6101
	$t_{1/2}$	hr	0.53	0.62	0.54	0.51
Liver	C_{max}	µg/mL	182	153	166	144
	T_{max}	hr	1	0.25	1	1
	AUC_{last}	µg•hr/mL	767	562	770	702
Brain	C_{max}	µg/mL	156	145	120	188
	T_{max}	hr	0.25	0.25	1	0.25
	AUC_{last}	µg•hr/mL	258	126	289	246

Table 3. Pharmacokinetics for HPβCD in plasma, liver, and brain tissues. C57BL/6J wild type mice were administered a single dose of vorinostat or TCF active and harvested 0.25, 1, 2, 4, or 7 hours post-injection. HPβCD drug levels were measured using LC-MS/MS. PK values were calculated from the average of n=4 mice per time point, and are shown for plasma, liver, and brain samples.

•3.3. Evaluation of efficacy of TCF formulation on lipid storage in liver tissue

To evaluate the efficacy of TCF, we conducted a short-term study in *Npc1*$^{I1061T/I1061T}$ mice. *Npc1*$^{I1061T/I1061T}$ mice harbor a point mutation in the NPC1 protein that models the most prevalent human NPC1 mutation, causing rapid ER-associated degradation of the misfolded protein [8, 22]. In cell-based models, HDACi have been shown to stabilize the NPC1I^{1061T} protein by facilitating its exit from the ER and targeting of the mutant, but correctly folded protein, to the lysosome, where it is functional [8, 21]. Therefore, the *Npc1*$^{I1061T/I1061T}$ mouse model is an ideal model to test proteostatic regulators, such as HDACi. Starting at four weeks of age, mice

were entered into a six-week treatment protocol, in which they were randomly allocated to one of nine treatment groups: PEG400/DMSO vehicle, HPβCD in water (CD/H_2O), HPβCD in vehicle (CD/Vehicle), HPβCD in water delivered 3x per week (CD/H_2O [3x/wk]), vorinostat, IVA, TCF active, TCF/IVA, and TCF/CI-994 (Table 1). CI-994 is a pan-HDAC inhibitor that has improved CNS penetration as compared to vorinostat. We reasoned that if TCF provides benefit by improving the ability of the HDACi to cross the blood brain barrier, a greater benefit might be seen with CI-994 than with vorinostat. Mice were treated weekly and euthanized at 10 weeks of age. Lipidomic profiling was performed to assess the effect of the formulations on lipid storage (Figure 2). We surveyed 42 sphingolipid and sterol species previously shown to be elevated in NPC1 mouse models and that respond to HPβCD treatment [34]. Significant reductions in lipid storage were observed in sterols (3β,5α,6β-cholestentriol and cholesterol), mono- and dihexosylceramides (MCer and DCer), and gangliosides (GA2, GM1 and GM2), and were limited almost exclusively to the treatment groups receiving HPβCD-containing formulations. By contrast, none of the treatment groups administered formulations containing vorinostat, CI994, or IVA alone showed evidence of lipid reduction, with the exception of a modest reduction in only a single lipid species (MCer 24:0) in the vorinostat group. We further assessed the effect of the different formulations on liver cholesterol by performing histochemical staining of liver sections from mice in the six-week trial using filipin, a fluorescent polyene antibiotic. Consistent with the lipidomic results, significant reduction in hepatocyte filipin staining (i.e., cholesterol storage) were found only in mice treated with HPβCD-containing formulations (Figure 3). These assessments focused on filipin staining of hepatocytes rather than Kupffer cells because HPβCD has previously been shown to reduce hepatocyte accumulation of cholesterol while enhancing storage in Kupffer cells [37]. Vorinostat in vehicle alone did not alter cholesterol levels. Taken together, these findings strongly support that the reduction in lipid storage is attributable to the actions of HPβCD rather than HDAC inhibition.

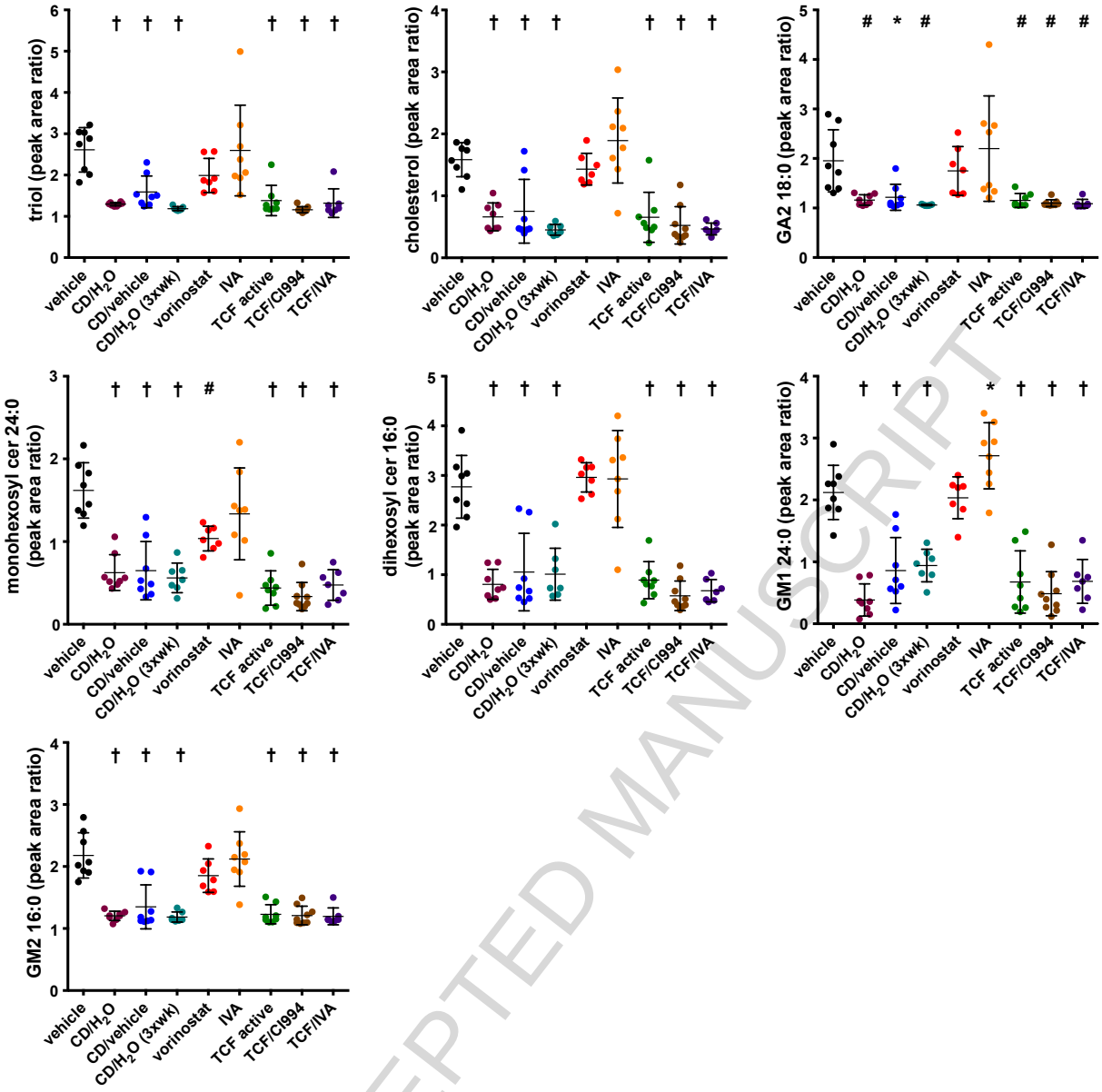

Figure 2. Lipidomics in liver tissue of *Npc1*$^{I1061T/I1061T}$ mice treated with TCF regimens. Beginning at four weeks of age *Npc1*$^{I1061T/I1061T}$ mice were treated weekly with one of the following regimens: vehicle (n=8), HPβCD in water (n=8), HPβCD in vehicle (n=8), vorinostat (n=7), inactive vorinostat (n=8), TCF active (n=8), TCF inactive (n=7), 4000mg/kg HPβCD in water delivered 3x/week (n=7), and TCF with CI-994 (n=9). After six weeks of treatment, animals were euthanized, liver tissue harvested, and lipid and sterol species quantified in liver homogenate using LC-MS/MS. Data for representative species are shown as mean ± SEM. Statistics were performed using ANOVA and significance determined versus vehicle using Dunnett's test. *, p<0.05; #, p<0.01; †, p<0.001.

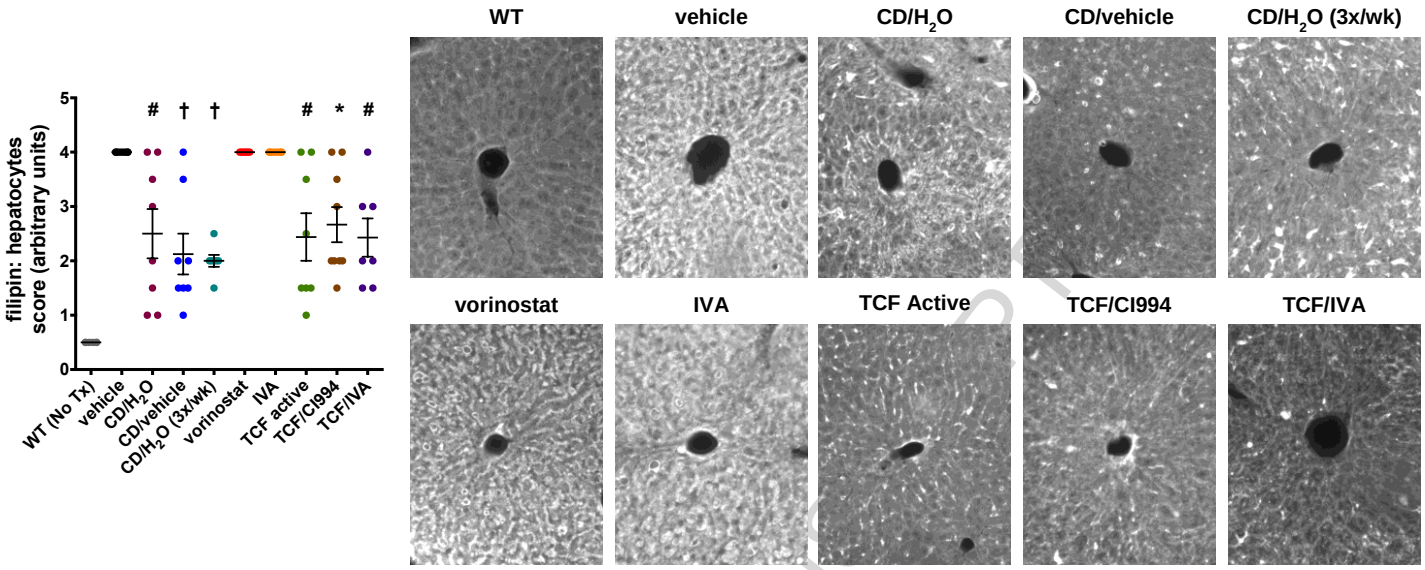

Figure 3. Filipin staining in liver tissue of *Npc1*$^{I1061T/I1061T}$ mice treated with TCF regimens. *Npc1*$^{I1061T/I1061T}$ mice were treated for six weeks with the various regimens as described in Figure 2 and liver tissue was analyzed for effect on cholesterol accumulation using filipin staining. Liver sections were analyzed in a blinded fashion on a scale of 0 – 5 (0 = no accumulation, 5 = extensive storage). Data are shown as mean ± SEM. Statistics were performed using ANOVA and significance determined using Dunnett's test. *, $p<0.05$; #, $p<0.01$; †, $p<0.001$. versus vehicle. Representative images (20x) are shown for all treatments.

3.4. Evaluation of efficacy of TCF formulation on lipid storage in brain tissue

39 sphingolipid and sterol species profiled in the liver were also measured in brain tissue (Figure 4). Significant reduction in 3β,5α,6β-cholestentriol, an established NPC1 disease marker, was observed in the HPβCD 3x/week, TCF active and TCF/CI994 groups. Reductions in GA2 ganglioside 18:0 and MCer 24:0 were also evident in the HPβCD 3x/week and TCF/CI994 groups. Overall, the effect of the different formulations on bulk lipid storage was less dramatic than in liver tissue both in the number of species affected and the magnitude of the responses. Selective examination of lipid storage in the cerebral cortex by immunohistochemical staining proved more sensitive, demonstrating decreased filipin and GM2 ganglioside staining in the HPβCD/vehicle, HPβCD 3x/week, and TCF active groups (Figure 5). No reductions were observed with the non- HPβCD containing formulations.

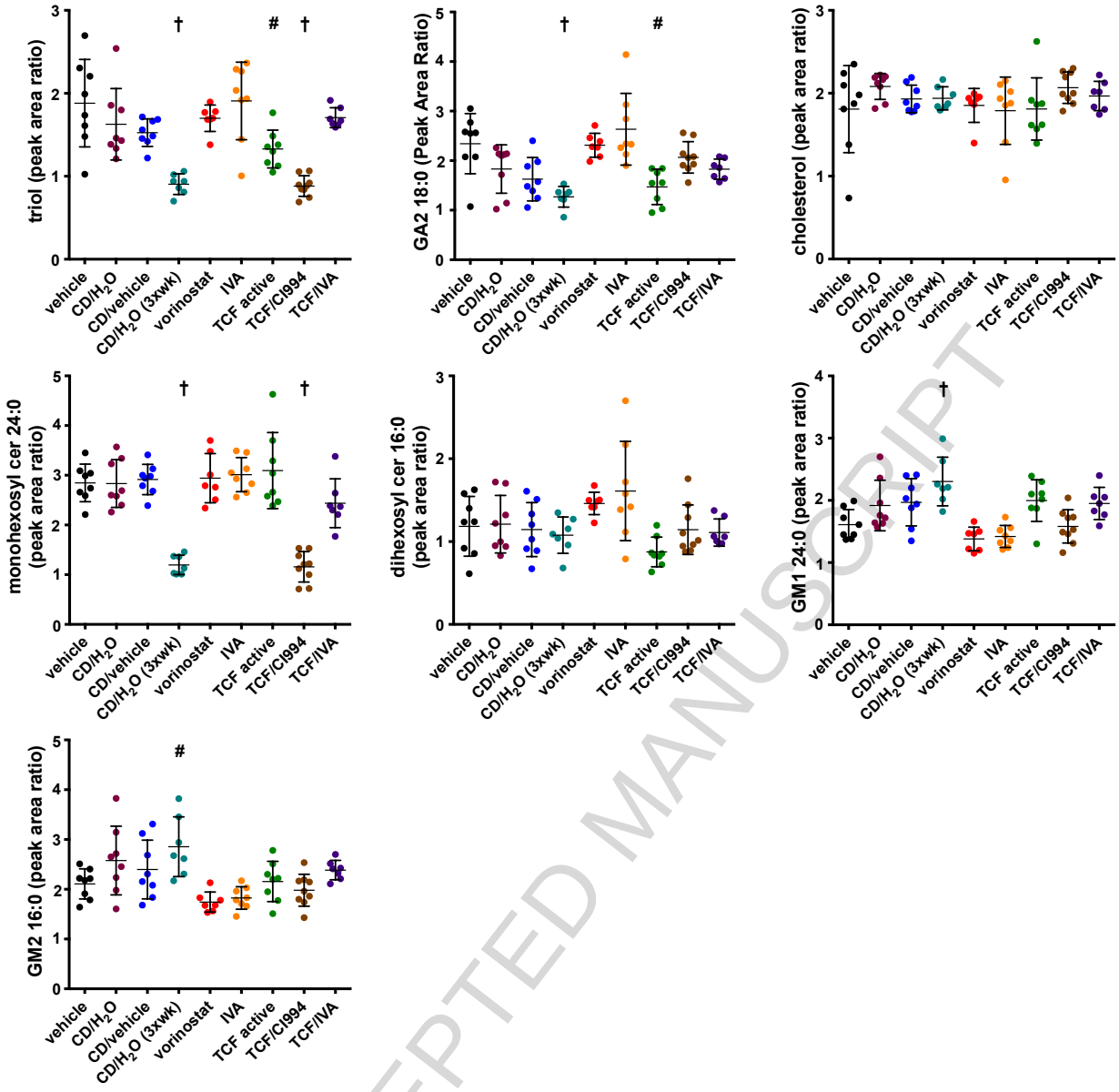

Figure 4. Lipidomics in brain tissue in *Npc1*$^{I1061T/I1061T}$ mice treated with TCF regimens. *Npc1*$^{I1061T/I1061T}$ mice were treated for six weeks with the various regimens as described in Figure 2, and lipid and sterol species were measured in brain homogenate using LC-MS/MS. Data for representative species are shown as mean ± SEM. Statistical analyses were performed by ANOVA and significance determined using Dunnett's test. #, $p<0.01$; †, $p<0.001$ with respect to vehicle.

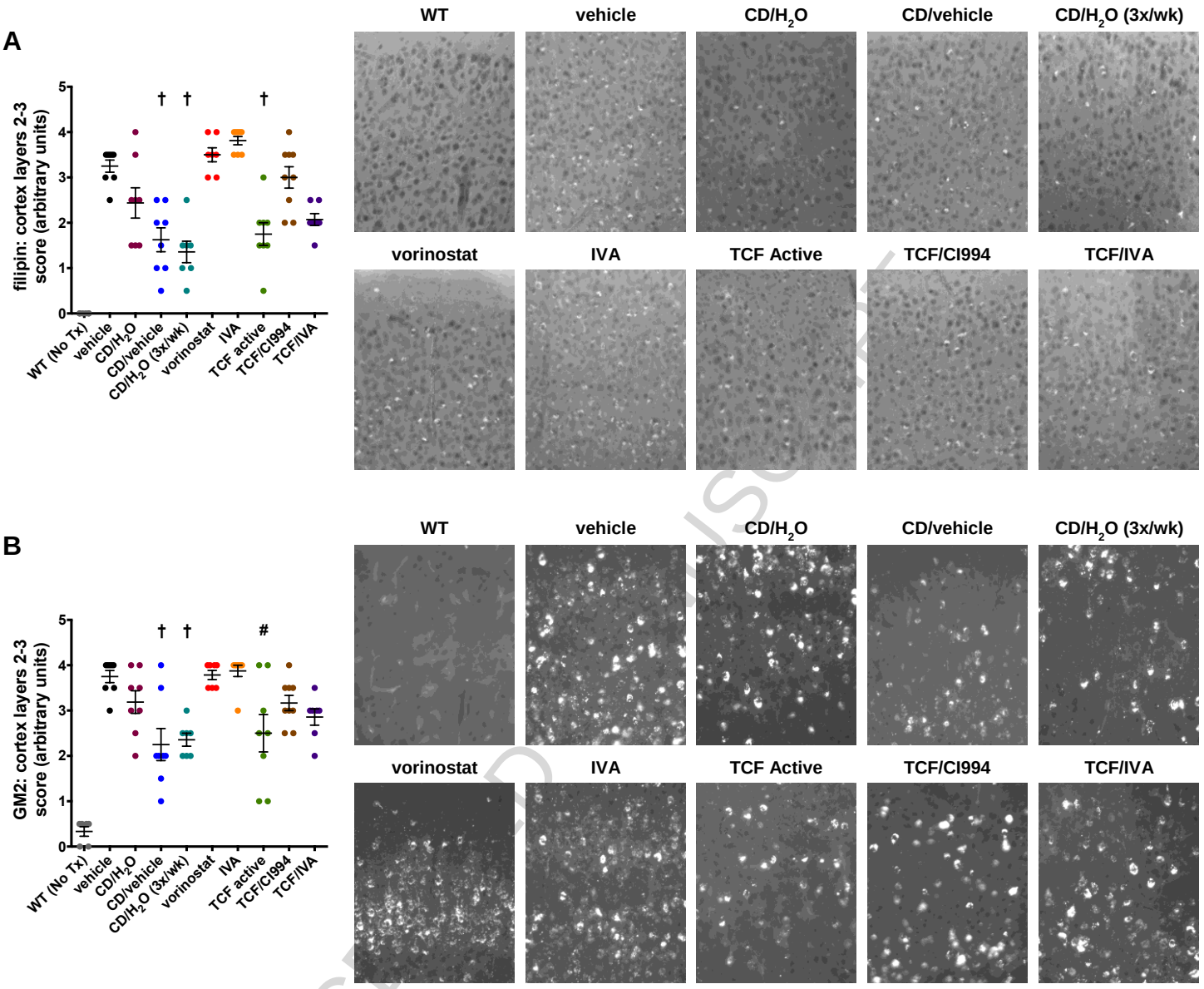

Figure 5. Filipin and GM2 ganglioside staining in cerebral cortex of *Npc1*$^{I1061T/I1061T}$ mice treated with TCF regimens. *Npc1*$^{I1061T/I1061T}$ mice were treated for six weeks with the various regimens as described in Figure 2, and neuropathology was assessed. (**A**) Filipin labeling of unesterified cholesterol and (**B**) immunoflourescent staining for GM2 ganglioside were performed on sections of the upper neocortex (layers 2-3). Representative images (20x) are shown for all. Samples were analyzed in a blinded fashion on a scale of 0 – 5 with (0 = no accumulation, 5 = extensive storage). All data are shown as mean ± SEM. Statistics were performed using ANOVA and significance determined using Dunnett's test. #, $p<0.01$; †, $p<0.001$ versus vehicle.

3.5. Effect of TCF formulations on histone acetylation

HDACi act by maintaining the acetylation levels of histones and non-histone proteins, such as molecular chaperones, by inhibiting their deacetylation by HDAC enzymes. This action could affect the proteostatic

environment of NPC1 protein [17, 38]. To examine the pharmacodynamic effect of the HDACi in the formulations, we determined the acetylation status of histone H3 in liver and brain tissues of the mice at the end of the six-week treatment trial (Figure 6). Samples were harvested one hour after the final dose, a time at which we previously had shown provides the maximal acetylation response. In liver, treatment with vorinostat, TCF active and TCF/CI994 resulted in a significant increase in the ratio of acetylated histone H3 relative to total histone H3 (Figure 6A), in agreement with the acute acetylation studies (Figure 1). In brain tissue, only vorinostat among the HDACi-containing formulations showed an increase in the ratio. The response for TCF active and TCF/CI994 was attenuated at 6 weeks, possibly due to less favorable PK in the setting of chronic administration. Unexpectedly, HPβCD 3x/week also showed an elevated ratio (Figure 6B). Since HPβCD did not increase H3 acetylation acutely (Figure 1), it is possible that the increased acetylation relates to the consequences of chronic administration of the drug and/or to changes in disease progression.

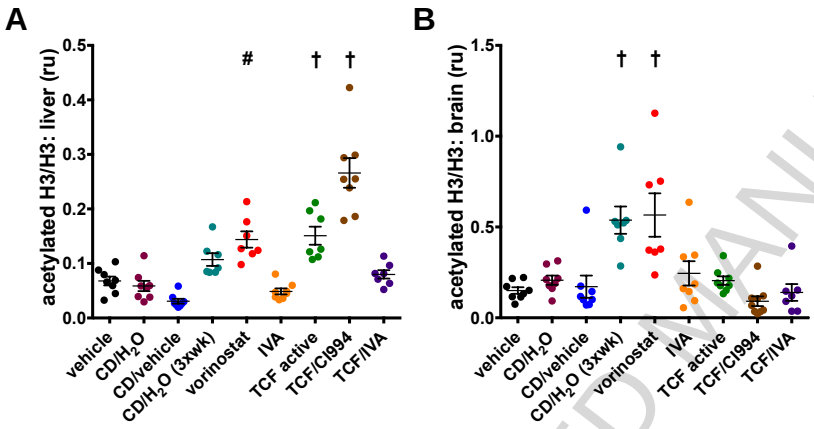

Figure 6. Histone H3 acetylation in brain tissue in *Npc1*$^{I1061T/I1061T}$ mice treated with TCF regimens. *Npc1*$^{I1061T/I1061T}$ mice were treated for six weeks with the various regimens as described in Figure 2, and acetylation of histone H3 was quantified via western blotting. In (**A**) liver and (**B**) brain, acetylated H3 and total H3 were normalized to the Hsp90 loading control, then taken as a ratio. Data are presented as mean ± SEM and statistical analysis was performed via ANOVA with Dunnett's test versus vehicle to determine significance. #, $p<0.01$; †, $p<0.001$.

3.6. Efficacy of TCF is independent of NPC1 protein expression

HDACi are hypothesized to reduce cholesterol storage in cells harboring NPC1 missense mutations by correcting NPC1 mutant protein misfolding, thereby facilitating the movement of the correctly folded but mutant protein to post-ER compartments. Although readily demonstrated in *Npc1*$^{I1061T/I1061T}$ fibroblasts [21, 22], whether this occurs *in vivo* is controversial [24, 26]. Here we performed western blot analysis of the NPC1I^{1061T} protein expression in liver and brain tissues from the mice treated with the TCF formulations (Figure 7). In none of the groups did we find evidence for stabilization of the mutant NPC1^{I1061T} protein in liver tissue; on the contrary, we observed reduction of NPC1 protein in CD/vehicle, CD/H_2O and vorinostat groups. In brain tissue, NPC1 protein was increased only in the CD/vehicle group, but not in mice treated with any of the HDACi-

containing formulations. Thus, there is no correlation between the efficacy of the formulations with respect to reduction in lipid storage and stabilization of the mutant NPC1^{I1061T} protein.

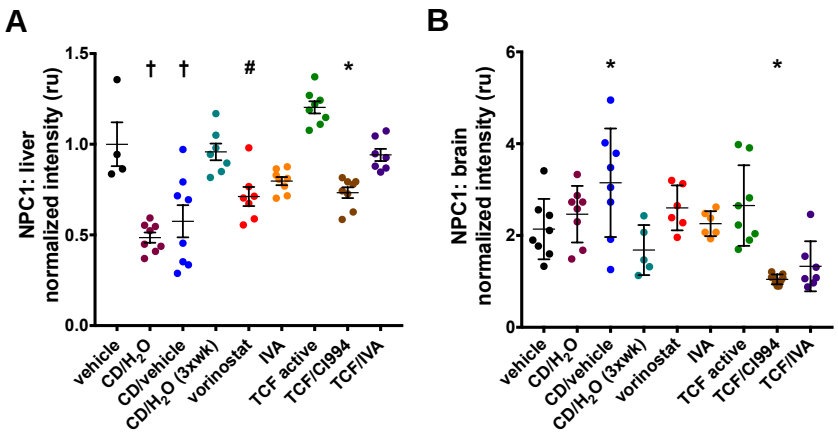

Figure 7. NPC1 Expression in liver and brain tissue in *Npc1*$^{I1061T/I1061T}$ mice treated with TCF regimens. *Npc1*$^{I1061T/I1061T}$ mice were treated for six weeks with the various regimens as described in Figure 2, and *Npc1*$^{I1061T/I1061T}$ mice (see Figure 2) by western blot analysis. (**A**) immunoprecipitations were performed in liver homogenates and samples were internally normalized to vehicle control after quantification. (**B**) SDS-PAGE and western blotting of membrane fractions isolated from brain. Samples were normalized to p63 loading control. Data are presented as mean ± SEM and statistical analysis was performed via ANOVA and significance determined using Dunnett's test. *, $p<0.05$; #, $p<0.01$; †, $p<0.001$ versus vehicle.

To further test the dependence NPC1 protein expression for the attenuation of lipid storage, we examined the effect of the formulations in *Npc1*$^{-/-}$ mice, which are null for NPC1 protein [29]. Four-week-old mice were randomly allocated to a six-week treatment protocol with PEG400/DMSO vehicle, CD/vehicle, or TCF active. The mice were treated weekly and euthanized at 10 weeks of age. Lipidomic profiling in liver (Figures 8) and brain tissue (Figure 9) was performed to assess the effect of the formulations on lipid storage. Both CD/vehicle and TCF active were equally effective in lowering lipid storage when compared to vehicle alone. Immunohistochemical staining of tissue sections showed reduced cholesterol staining in liver (Figure 10A) and cerebral cortex (Figure 10B) for both groups, as well as reduced GM2 ganglioside staining in cortex for the TCF active group (Figure 10C). Taken together with the unchanged NPC1 protein expression, these findings indicate that reduction in lipid storage resulting from the TCF formulations is independent of NPC1 proteostatic regulation.

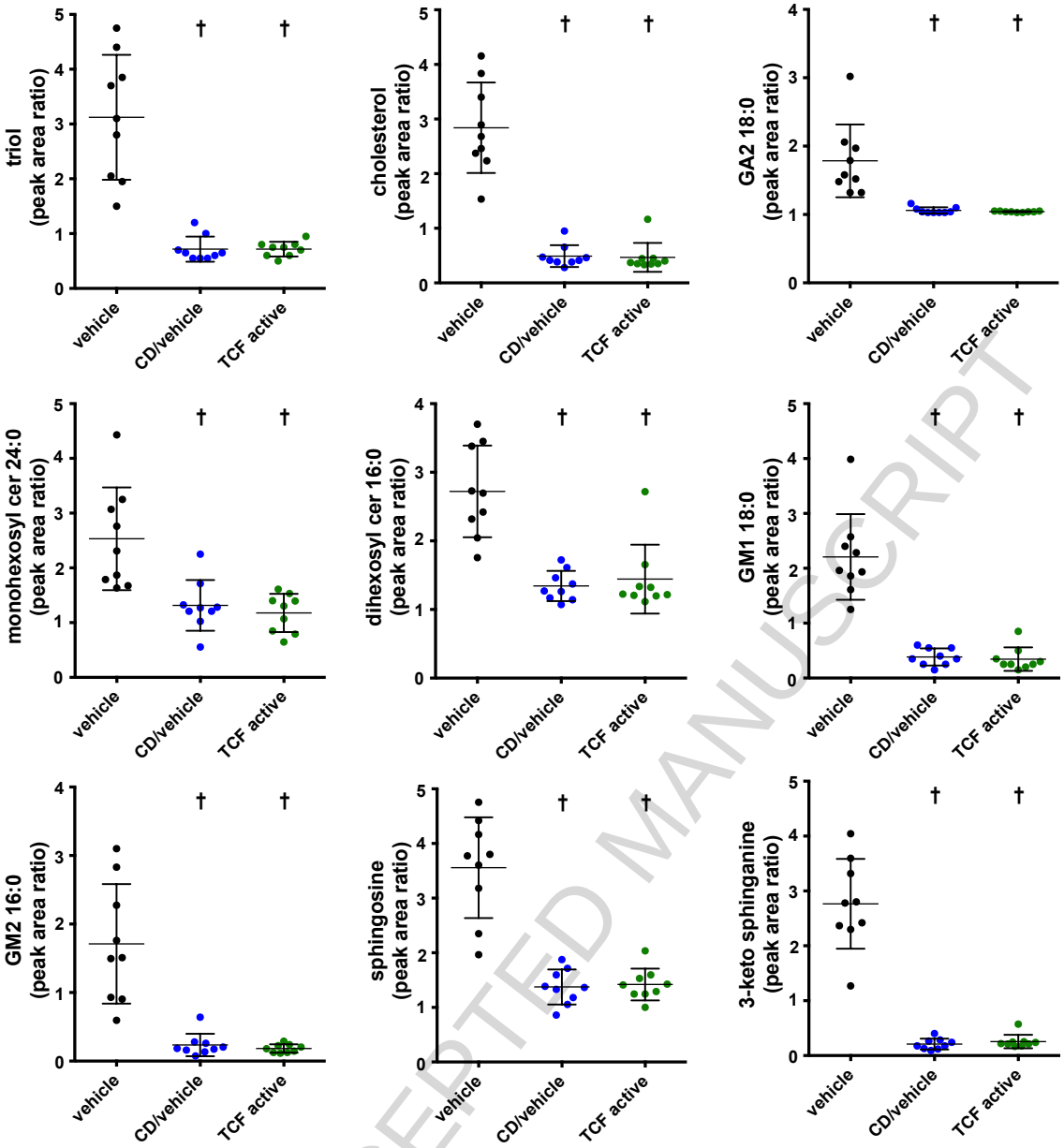

Figure 8. Lipidomics in liver tissue in *Npc1*$^{-/-}$ mice treated with TCF regimens. *Npc1*$^{-/-}$ mice were treated for six weeks with PEG/DMSO vehicle (n=9), 2000mg/kg HPβCD in water (n=9), TCF with vorinostat (n=9), or untreated (n=8). Lipid and sterol species were measured in liver homogenate using LC-MS/MS. Data for representative species are reported as mean ± SEM. Statistical analyses were performed by ANOVA and significance determined using Dunnett's test. †, $p<0.001$ versus vehicle.

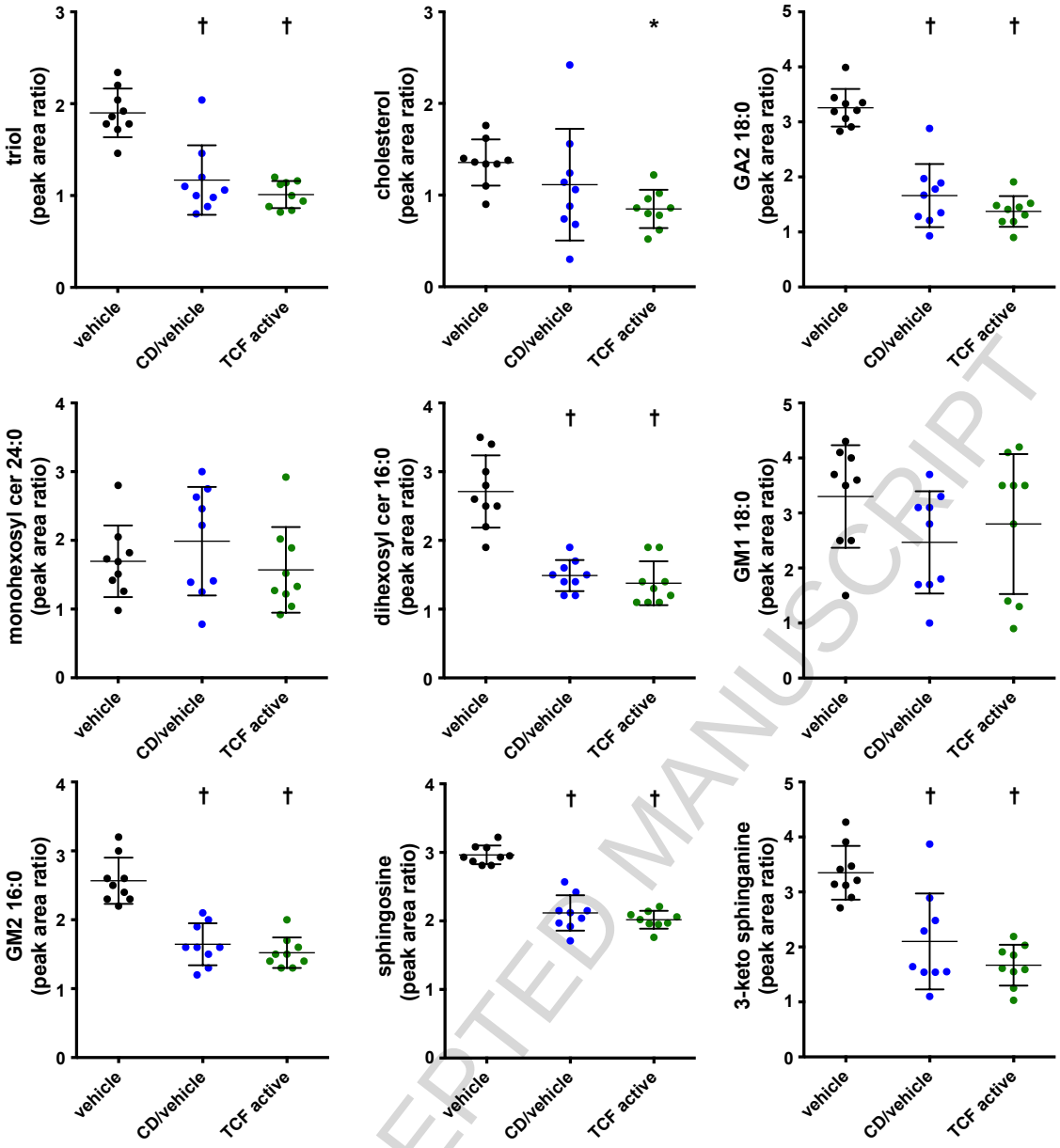

Figure 9. Lipidomics in brain tissue in *Npc1*$^{-/-}$ mice treated with TCF regimens. *Npc1*$^{-/-}$ mice were treated for six weeks with the various regimens as described in Figure 8. Lipid and sterol species were measured in brain homogenate using LC-MS/MS. Data for representative species are reported as mean ± SEM.Statistical analyses were performed by ANOVA and significance determined using Dunnett's test. *, $p<0.05$; †, $p<0.001$ versus vehicle.

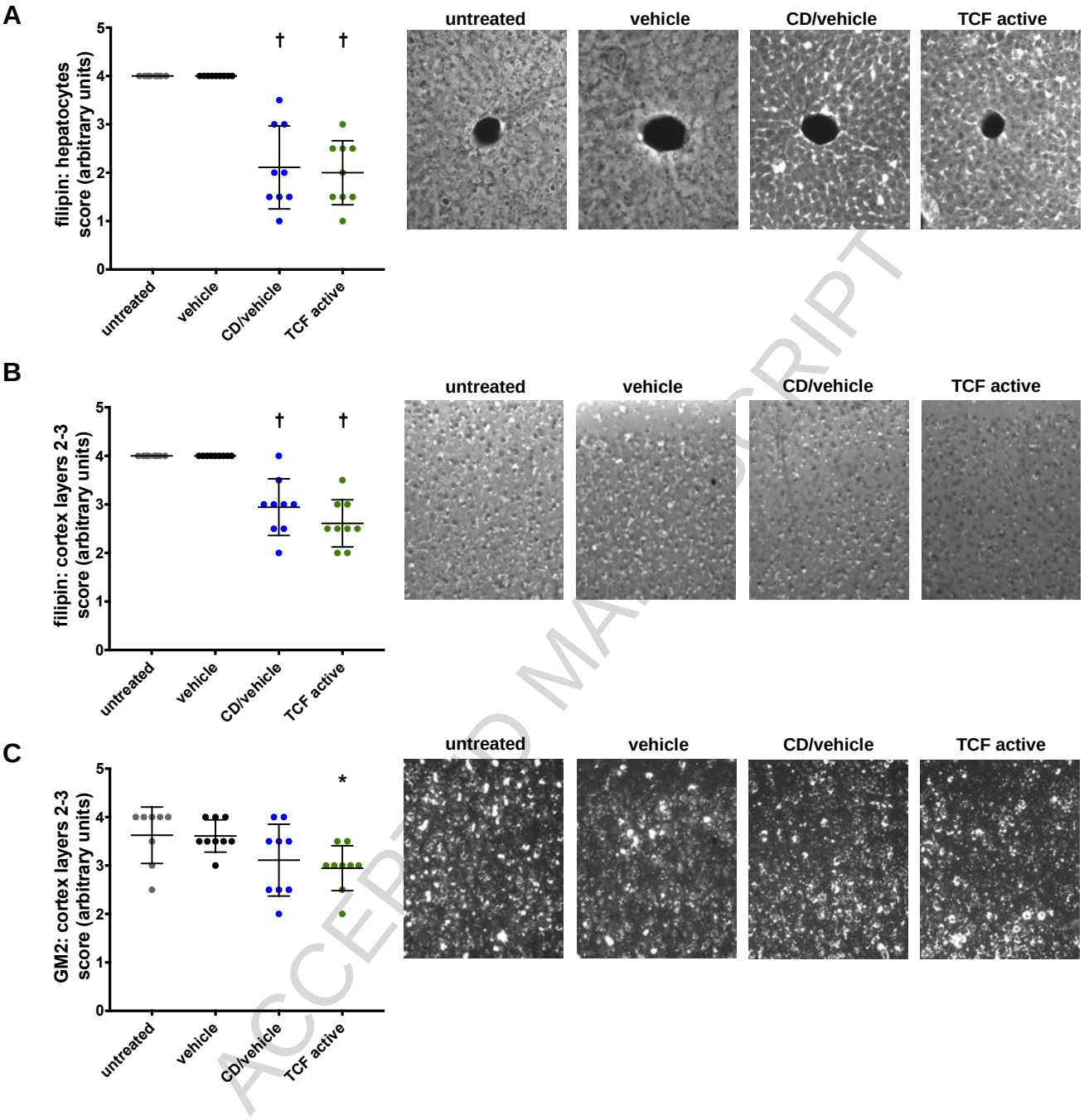

Figure 10. Filipin and GM2 ganglioside staining in liver and cerebral cortex of *Npc1*$^{-/-}$ mice treated with TCF regimens. *Npc1*$^{-/-}$ mice were treated for six weeks with the various regimens as described in Figure 8. Unesterified cholesterol in (**A**) hepatocytes and (**B**) upper neocortex sections were detected by filipin staining and analyzed in a blinded fashion on a scale of 0 – 5 with (0 = no accumulation, 5 = extensive storage). (**C**) Immunofluorescence staining for GM2 ganglioside was performed on the upper neocortex and analyzed in the same manner. Data are shown as mean ± SEM. Statistics performed using ANOVA and Dunnett's test to determine significance versus vehicle control. *, $p<0.05$; †, $p<0.001$. Representative images (20x) are shown.

3.7. Effect of TCF on neurological function and survival of the *Npc1*$^{I1061T/I1061T}$ mice

To determine whether the results from short-term treatment trials correlated with survival in the *Npc1*$^{I1061T/I1061T}$ mouse model, mice were randomly allocated to one of nine treatment groups (Table 1). Untreated wild type mice and *Npc1*$^{I1061T/I1061T}$ mice served as controls. Starting at four weeks, mice in the treatment groups were treated weekly (with the exception of the 3x/week HPβCD) with one of the nine regimens. Mice were terminated when they showed clinical signs of end-stage disease [10]. Weekly weights plotted versus time show a clear separation of groups receiving HPβCD-containing formulations (red lines) versus groups receiving formulations without HPβCD (blue lines) (Figure 11). The median survival for all groups receiving HPβCD-containing formulations, including TCF/IVA, were significantly increased compared to either untreated mutant mice or mice treated with the PEG400/DMSO vehicle (Figure 12). As expected, treatment with HPβCD 3x/week resulted in the longest median survival. Neither vorinostat nor IVA extended lifespan.

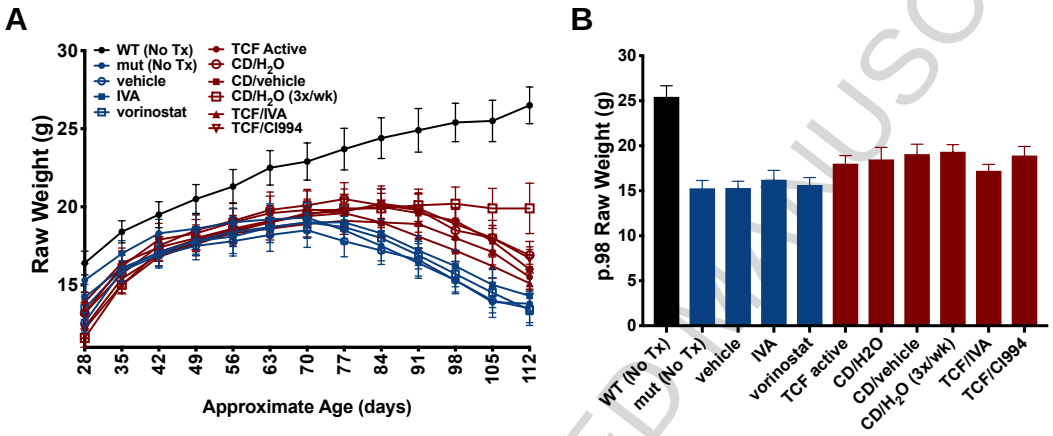

Figure 11. Growth curves for *Npc1*$^{I1061T/I1061T}$ mice in TCF treatment survival study. (A) Weights of wild type (WT) and *Npc1*$^{I1061T/I1061T}$ mice treated with the indicated regimens beginning at 4 weeks were recorded weekly (n=4 for HPβCD administered 3x/week, all other regimens n=8). For survival study, mice were euthanized when they showed clinical signs of end-stage disease. (B) Body weight distribution of mice in survival study at p.98. Data are displayed as mean ± SEM, and are color-coded (WT, black; non-HPβCD containing formulas, blue; and HPβCD-containing formulas, red).

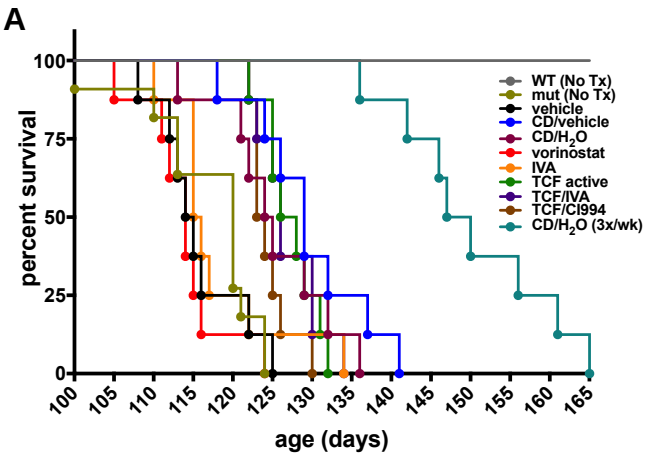

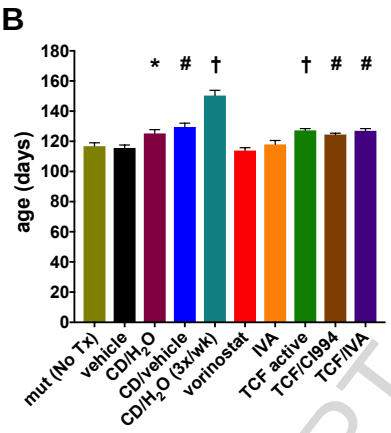

C

Treatment Group	Mean Lifespan (days)	Median Lifespan (days)
WT	342.6	364.0
Mutant	116.8	120.0
vehicle	115.6	114.5
CD/H_2O	125.2	124.5
CD/vehicle	129.5	129.0
CD/H_2O (3x/wk)	150.4	148.5
vorinostat	113.8	114.0
IVA	118.0	115.5
TCF active	127.2	127.0
TCF/CI994	124.5	123.5
TCF/IVA	127.0	126.0

Figure 12. Survival for *Npc1*$^{I1061T/I1061T}$ mice in TCF treatment survival study. (**A**) Kaplan-Meier survival curves were generated for *Npc1*$^{I1061T/I1061}$ mice treated weekly with the indicated regimens beginning at 4 weeks. (**B**) Average lifespan for each group are shown mean ± SEM. Statistical significance was determined by unpaired t-test with Welch's correction in comparison to NPC1^{I1061T} mice (mut (No Tx)). *, p<0.0332; #, p<0.0021; †, p<0.0002. (**C**) Mean and median lifespan for each treatment group.

We further examined the effect of the TCF formulations on the neurological disease progression in the mice using automated gait analysis, which has been previously validated in NPC1 mouse models [39]. Gait analysis was performed weekly during the survival study. Results are shown for standing on the diagonal, right front-right hind leg coupling, and forepaw stride length at 4 weeks (pre-treatment), 8 weeks and 12 weeks of age (Figure 13 and Supplemental Movie 1). At 12 weeks, the untreated and vehicle-treated *Npc1*$^{I1061T/I1061T}$ mice have profound deficits in standing on the diagonal, as compared to wild type mice. There is, however, significant preservation of function in all of the groups receiving formulations containing cyclodextrin and PEG400/DMSO vehicle (CD/H2O treatment group shows a trend (p=0.0767) compared to vehicle). Similar results were obtained for analysis of forepaw stride length, and to a lesser extent with the right front-right hind leg coupling. Together, these finding demonstrate that the survival benefit and preservation of neurological function in the treated mice derive exclusively from HPβCD exposure and not from the inclusion of HDACi in the TCF. Moreover, the concordance between results from the six week studies and the survival studies

provide validation for use of the short-term treatment paradigm to evaluate drug therapies in the *Npc1*$^{I1061T/I1061T}$ mouse model.

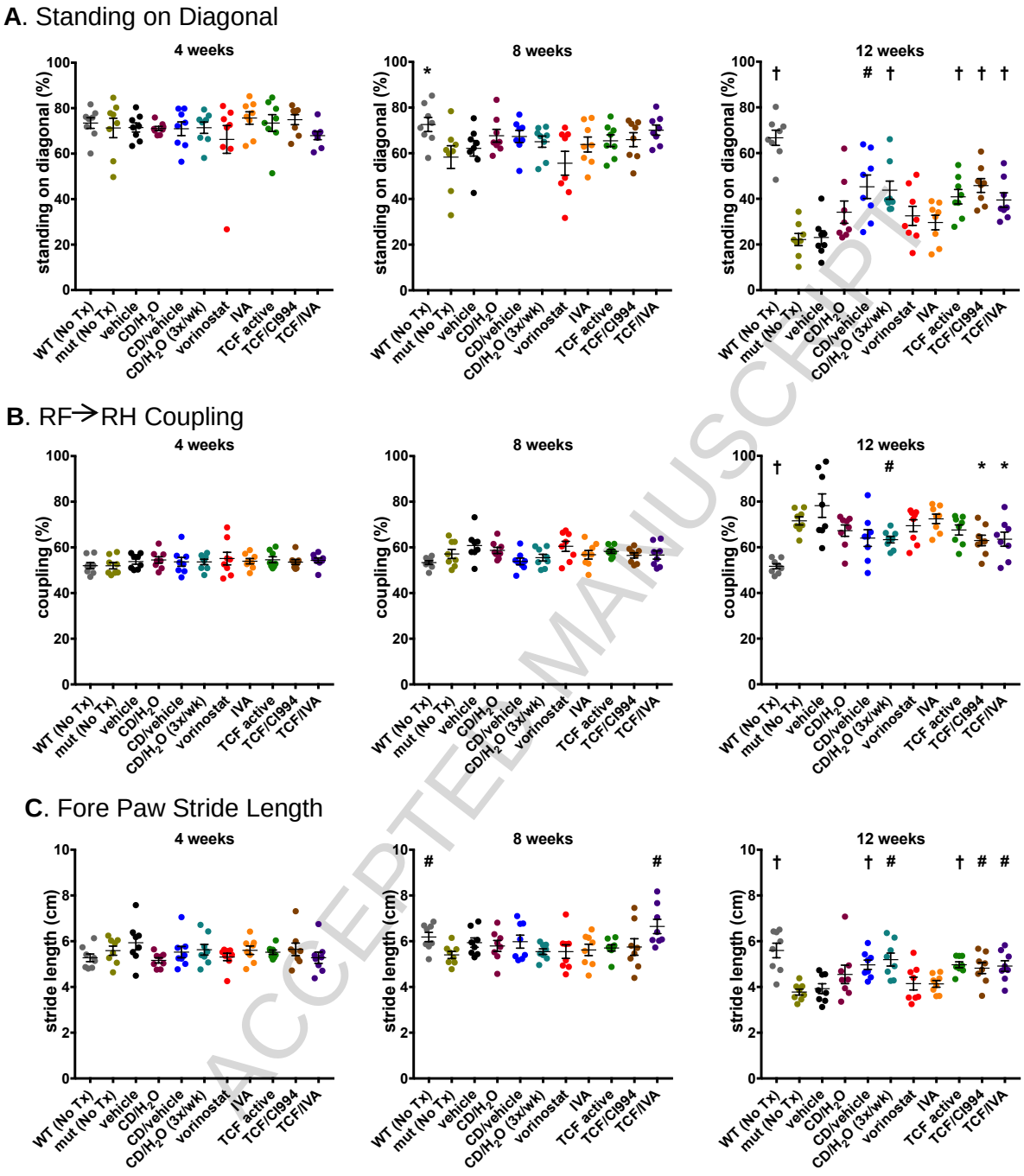

Figure 13. Gait analysis for *Npc1*$^{I1061T/I1061T}$ mice in TCF treatment survival study. Gait analysis data was performed weekly to monitor cerebellar function in *Npc1*$^{I1061T/I1061}$ mice treated with various regimens described in Figure 2. (**A**) Standing on Diagonal, (**B**) right forepaw to right hindpaw coupling, and (**C**) forepaw stride length are shown at three representative time points representative of different stages of disease progression in the *Npc1*$^{I1061T/I1061}$ mice: 4 weeks (pre-symptomatic), 8 weeks (onset of symptoms), 12 weeks (late stage disease). Data are displayed as mean ± SEM. Statistical analysis was performed using unpaired t-tests with Welch's correction. *, p<0.0332; *#, p<0.0021; †, p<0.0002; versus untreated mutant.

3.8. Lack of efficacy of HDACi in bone marrow-derived macrophages

One possible explanation for the lack of efficacy of vorinostat in *Npc1*$^{I1061T/I1061T}$ mice while there is a robust effect in tissue culture cells is that most cell populations *in vivo* are slowly dividing as compared to rapidly dividing cells in tissue culture. The effect of vorinostat was tested on slowly dividing terminally differentiated bone marrow-derived macrophages. BMMs were treated with vorinostat at eight different doses ranging from 4 nM to 10 µM for 48h or 72h, and the level of cholesterol accumulation in LSOs was measured using a filipin imaging assay that measures cholesterol in LSOs, which accumulate near the center of NPC1 mutant cells (Figure 14) [20, 21]. Vorinostat treatment was toxic to BMMs at concentrations above 1 µM. Each data point in the plot shown in the figure, is normalized to corresponding DMSO treated cells. Hence, the value of one indicates no correction. Although, 330 nM treatment showed slight decrease in cholesterol accumulation based on filipin intensity, it was not as robust as the response observed in NPC1^{I1061T} fibroblasts. Thus, vorinostat is not effective at reducing the cholesterol accumulation in slowly dividing, differentiated macrophages.

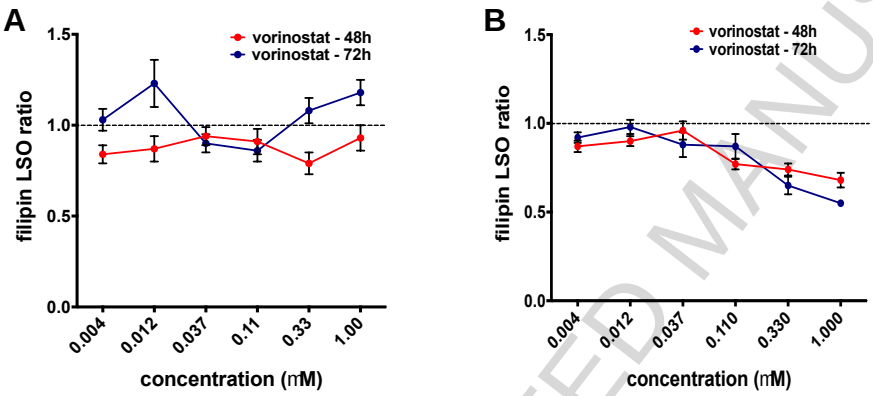

Figure 14. Vorinostat does not reduce cholesterol storage in ex vivo bone marrow-derived macrophages. (**A**) Differentiated BMMs and (**B**) *Npc1*$^{I1061T/I1061T}$ human fibroblasts were plated in 384 well plates and incubated overnight. Cells were then treated with various doses (4-6 wells per dose) and incubated for an additional 48 or 72 hours. For the final 24 hours the medium was supplemented with 20 µg/ml acetylated LDL to increase cholesterol loading. Finally, the cells were washed with PBS, fixed with 2% PFA and stained with filipin and Draq5. Four fluorescence images per well were acquired. Images were analyzed to measure filipin intensity in lysosome like organelles (LSO) per cell. The LSO ratios in vorinostat treated cells were normalized to corresponding DMSO treated cells. Hence, LSO values less than one indicate reduction of stored cholesterol. Each data point is an average from 2-5 independent experiments and total of 48-80 images. Although the 330 nM treatment at 48h showed a slight decrease in cholesterol accumulation in BMMs, it did not achieve significance when corrected for multiple pair-wise comparisons. Error bars ± SEM.

4. DISCUSSION

In cell-based assays HDACi have shown promise for correction of the lipid storage caused by NPC1 deficiency [19-21], but there are conflicting reports as to whether HDACi are able to mitigate the NPC1 phenotype *in vivo*

[24, 26, 27]. In the present study we examined the efficacy of HDACi in the context of TCF in *Npc1*$^{I1061T/I1061T}$ mice. Although we found that TCF containing vorinostat was effective in delaying neurodegeneration in the NPC1 mice, TCF containing the inactive form of vorinostat was equally efficacious, clearly demonstrating that the benefit of TCF was independent of HDACi activity. Instead, we show that efficacy of TCF was attributable to enhanced PK of the HPβCD component in the formulation. While we acknowledge that differences between the *Npc1*$^{I1061T/I1061T}$ and *Npc1*^{nmf164} models may account for differences in pharmacokinetic findings, the TCF was similarly efficacious in the NPC1-null BALB/c *Npc1*^{nih} mice, indicating that the benefit of TCF was independent of NPC1 gene and protein expression or strain differences. Furthermore, HDACi were ineffective in alleviating cholesterol storage in primary bone marrow derived macrophages from *Npc1*$^{I1061T/I1061T}$ mice, suggesting that this therapeutic paradigm may not be applicable to slowly dividing cells. Taken together, these findings provide an explanation for the lack of benefit of HDACi *in vivo* in the absence of the HPβCD carrier [24, 26, 27].

As the neuroprotective benefits of HPβCD in NPC1 disease models are well established [10-12], its inclusion in TCF presents a major confounder for interpretation of the formulation's efficacy [26]. The goal of our study was not a precise replication of the experiments by Alam and colleagues, but to test which component or interaction of the TCF was responsible for the mitigation of the NPC phenotype. In order to deconvolute the effects of HPβCD from the other TCF components, we rigorously examined the impact of TCF on the PK each of the components. We excluded day 7 and day 15 HPβCD pretreatment of the TCF group, a potential confounder, and included a key control, HPβCD in PEG/DMSO vehicle. We found that the benefits of TCF with respect to reduction of lipid storage in brain tissue and prolonged survival in the *Npc1*$^{I1061T/I1061T}$ mice could be predicted solely on the basis of the PK properties of HPβCD in the different formulations. Inclusion of the PEG400/DMSO co-solvents reduced renal clearance and markedly enhanced the plasma and tissue AUC_{last} for HPβCD, as compared to water vehicle. Not only was HPβCD in PEG/DMSO vehicle more efficacious than HPβCD in water, but it was also equally efficacious to TCF containing HDACi. Thus, we conclude that the active component in TCF is the HPβCD and that the PEG/DMSO vehicle simply enhanced its pharmacokinetics.

Although our vorinostat PK analysis was consistent with the previous report by Alam and colleagues – TCF increased the vorinostat C_{max} and AUC_{last} in brain tissue by 55% and 50%, respectively – the increased survival of TCF-treated NPC1 mice, as noted above, was independent of the pharmacokinetics and activity of the HDACi. It is unclear how HPβCD increased brain exposure of vorinostat, but could relate to cyclodextrin's known ability to inhibit P-glycoprotein (P-gp)-mediated efflux of drugs across the blood-brain barrier [40]. By including an IVA control in our study, we excluded a role for HDAC inhibition since substitution of inactive for the active form of vorinostat in the TCF had no impact on its efficacy. Furthermore, we found no evidence of increased HDACi activity in brain tissue in the context of chronic delivery (Alam et al. reported increased HDACi activity in brain tissue but only following acute TCF administration). Together, these findings argue

strongly that the efficacy of TCF is neither dependent on the presence of vorinostat nor requires its HDACi activity.

HDACi are proposed to correct the NPC1 phenotype through proteostatic regulation of the mutant NPC1 protein [8, 19-21], possibly via transcriptional upregulation of the NPC1 gene [26] and/or of endogenous molecular chaperones [17]. Indeed, in cell-based models, vorinostat has been shown to prolong the half-life of the mutant NPC1^{I1061T} protein, which is normally rapidly degraded [21]. In the present study, however, none of the formulations examined led to an increase in NPC1^{I1061T} protein expression in either liver or brain tissue. This is consistent with an earlier report by Munkacsi and colleagues using the NPC1^{nmf164} mice [24], though differs from Alam and colleagues who showed increased NPC1 mutant protein in the same mouse model [26]. To directly address the requirement for NPC1 mutant protein expression for TCF efficacy, we treated NPC1^{nih} mice that are null for NPC1 protein with the formulations. We found that both TCF active vorinostat and HPβCD in PEG/DMSO vehicle attenuated lipid storage in liver and brain tissue, and that these formulations were equally efficacious. Thus, we conclude that the benefit conferred by TCF in the NPC1 mouse models is independent of NPC1 protein expression.

Previous studies have shown that HDAC inhibition alleviates cholesterol storage in a variety of NPC1-deficient cell lines, including patient fibroblasts and murine embryonic fibroblasts from the *Npc1*$^{I1061T/I1061T}$ mice [19-22]. Nevertheless, translation of the findings from cultured cells to *in vivo* NPC1 mouse models has been elusive [24, 26]. In the present study we show that treatment with HDACi failed to reduce cholesterol storage *ex vivo* in bone marrow-derived macrophages harvested from *Npc1*$^{I1061T/I1061T}$ mice. While the explanation for these divergent findings is uncertain, the absence of response to HDAC inhibition may reflect the fact that bone marrow-derived macrophages are slowly dividing or post-mitotic whereas cultured fibroblasts are actively dividing. It seems plausible that HDACi might be more effective in actively dividing cells with more open chromatin than in non-dividing cells with more condensed chromatin [41]. This is consistent with the clinical use of HDACi for treatment of cancers, and would potentially explain the failure of vorinostat to mitigate lipid storage in liver tissue, even when tissue levels are at the EC_{50} for the drug [24].

The finding that PEG400 enhanced HPβCD exposure in brain tissue begs the question as to whether the addition of the co-solvent to HPβCD formulations might offer intravenous delivery as an alternative to the current more invasive intrathecal approach [13]. Our PK studies showed that HPβCD in the PEG400/DMSO achieved roughly twice the brain exposure of HPβCD in water. Therefore, even in the setting of a peripheral dose of 4000 mg/kg HPβCD – a dose that is toxic in the NPC1 cat model and cannot be safely delivered in humans [11] – the maximum drug concentration achieved would be ~15 μM [16]. This is well below the 1000 μM drug concentration achieved in CSF following direct CNS administration of HPβCD [31], suggesting that

the addition of PEG400 to an intravenous HPβCD formulation is unlikely to circumvent the requirement for intrathecal delivery.

Finally, an important contribution of the present study is the validation of a short-term treatment regimen for drug screening in the *Npc1*$^{I1061T/I1061T}$ mice. Through application of broad targeted lipidomics, we developed a set of lipid biomarkers that are highly sensitive indicators of NPC1 disease and response to treatment. We found that coupling measurement of the set of curated lipid biomarkers in brain and liver tissue with quantitative immunohistochemical assessment of cholesterol and GM2 ganglioside storage in cerebral cortex was highly predictive of the effects of treatment regimens on both neurological function and survival. Thus, the six-week treatment paradigm offers a rapid and cost-effective approach to drug discovery and in vivo screening for NPC1 disease.

ACKNOWLEDGEMENTS

Funding: This work was supported by grants from the Ara Parseghian Medical Research Fund (P.H., O.W., G.L., F.S., B.J.M., D.S.O., S.U.W. and F.R.M), NIH Grant R01 NS092653 (P.H., O.W., D.S.O., S.U.W. and F.R.M), and NSF grants CHE-1058075 and CHE-1565669 (M.G.). This study was also supported by the intramural research program of the *Eunice Kennedy Shriver* National Institute of Child Health and Human Development (F.D.P.). This work was performed in the Metabolomics Facility at Washington University (NIH P30 DK020579 and NIH P30 DK056341). **Author contributions**: J.D., E.Q., S.M., J.Z. and S.E.G. performed the mouse studies. X.J., R.S., J.Z., P.K. and H.F. performed mass spectrometry experiments and analyzed and interpreted the data. X.X. performed the PK analyses. C.D. and S.U.W. performed histopathology and analyzed the data. M.G., G.L. and F.S. performed the syntheses of compounds and internal standards under the direction of P.H. and B.J.M. K.S. and N.P. assisted with analysis of histone acetylation. O.W., P.H., E.H., F.D.P., S.U.W., F.R.M., J.E.S. and D.S.O. planned the studies and wrote the manuscript. **Competing interests**: The authors report no competing interests. **Data and materials availability**: All reasonable requests for chemical compounds and assay protocols described in this work will be fulfilled via an MTA or licensing agreements with the University of Notre Dame or Washington University.

SUPPLEMENTARY MATERIALS

PEG Pharmacokinetic Parameters								
			Treatment					
			vehicle	CD/vehicle	vorinostat	IVA	TCF active	TCF/IVA
Matrix	Parameters	Unit						
Liver	T_{max}	hr	0.25	1	1	0.25	1	0.25
	C_{max}	µg/g	605	952	906	945	1343	789
	AUC_{last}	µg•hr/g	1329	1713	2036	1669	3042	1787
	AUC_{inf}	µg•hr/g	1358	1787	2157	1694	3064	1899
	AUC_{extrap}	%	2.15	4.12	5.60	1.48	0.74	5.89
	$t_{1/2}$	hr	0.677	0.787	0.903	0.628	0.930	0.937
Brain	T_{max}	hr	1	0.25	2	0.25	2	1
	C_{max}	µg/g	119	170	128	126	152	143
	AUC_{last}	µg•hr/g	390	737	691	530	808	734
	AUC_{inf}	µg•hr/g	NC	1095*	NC	1050*	NC	1000
	AUC_{extrap}	%	NC	32.8*	NC	49.5*	NC	26.6
	$t_{1/2}$	hr	NC	4.24	NC	6.59	NC	3.80

Supplemental Table 1. Pharmacokinetics for PEG400 in plasma, liver, and brain tissues. C57BL/6J wild-type mice were given a single dose of vehicle, cyclodextrin in vehicle, vorinostat, inactive vorinostat, TCF active, or TCF/IVA and harvested 0.25, 1, 2, 4, or 7 hours post-injection. PEG concentrations were measured using LC-MS/MS in both brain and liver homogenates. PK values were calculated from the average of n=4 mice per time point and are shown for plasma, liver, and brain samples. NC: Not calculated due to a flat curve in the terminal phase. *Calculated AUC_{inf} value less certain since the extrapolated AUC was > 30.

Supplemental Movie 1. Representative videos used for gait analysis of 12 week old mice in treatment groups

REFERENCES AND NOTES

[1] M.T. Vanier, Niemann-Pick disease type C, Orphanet J Rare Dis, 5 (2010) 16.

[2] E.D. Carstea, J.A. Morris, K.G. Coleman, S.K. Loftus, D. Zhang, C. Cummings, J. Gu, M.A. Rosenfeld, W.J. Pavan, D.B. Krizman, J. Nagle, M.H. Polymeropoulos, S.L. Sturley, Y.A. Ioannou, M.E. Higgins, M. Comly, A. Cooney, A. Brown, C.R. Kaneski, E.J. Blanchette-Mackie, N.K. Dwyer, E.B. Neufeld, T.Y. Chang, L. Liscum, J.F. Strauss, 3rd, K. Ohno, M. Zeigler, R. Carmi, J. Sokol, D. Markie, R.R. O'Neill, O.P. van Diggelen, M. Elleder, M.C. Patterson, R.O. Brady, M.T. Vanier, P.G. Pentchev, D.A. Tagle, Niemann-Pick C1 disease gene: homology to mediators of cholesterol homeostasis, Science, 277 (1997) 228-231.

[3] S. Naureckiene, D.E. Sleat, H. Lackland, A. Fensom, M.T. Vanier, R. Wattiaux, M. Jadot, P. Lobel, Identification of HE1 as the second gene of Niemann-Pick C disease, Science, 290 (2000) 2298-2301.

[4] R.E. Infante, M.L. Wang, A. Radhakrishnan, H.J. Kwon, M.S. Brown, J.L. Goldstein, NPC2 facilitates bidirectional transfer of cholesterol between NPC1 and lipid bilayers, a step in cholesterol egress from lysosomes, Proc Natl Acad Sci U S A, 105 (2008) 15287-15292. https://doi.org/0807328105 [pii]
10.1073/pnas.0807328105

[5] H.J. Kwon, L. Abi-Mosleh, M.L. Wang, J. Deisenhofer, J.L. Goldstein, M.S. Brown, R.E. Infante, Structure of N-terminal domain of NPC1 reveals distinct subdomains for binding and transfer of cholesterol, Cell, 137 (2009) 1213-1224. https://doi.org/S0092-8674(09)00393-6 [pii]
10.1016/j.cell.2009.03.049

[6] D.S. Ory, Niemann-Pick type C: a disorder of cellular cholesterol trafficking, Biochim Biophys Acta, 1529 (2000) 331-339.

[7] G. Millat, C. Marcais, M.A. Rafi, T. Yamamoto, J.A. Morris, P.G. Pentchev, K. Ohno, D.A. Wenger, M.T. Vanier, Niemann-Pick C1 disease: the I1061T substitution is a frequent mutant allele in patients of Western European descent and correlates with a classic juvenile phenotype, Am J Hum Genet, 65 (1999) 1321-1329.

[8] M.E. Gelsthorpe, N. Baumann, E. Millard, S.E. Gale, S.J. Langmade, J.E. Schaffer, D.S. Ory, Niemann-Pick Type C1 I1061T Mutant Encodes a Functional Protein That Is Selected for Endoplasmic Reticulum-associated Degradation Due to Protein Misfolding, J Biol Chem, 283 (2008) 8229-8236.

[9] M.C. Patterson, D. Vecchio, H. Prady, L. Abel, J.E. Wraith, Miglustat for treatment of Niemann-Pick C disease: a randomised controlled study, Lancet Neurol, 6 (2007) 765-772.

[10] C.D. Davidson, N.F. Ali, M.C. Micsenyi, G. Stephney, S. Renault, K. Dobrenis, D.S. Ory, M.T. Vanier, S.U. Walkley, Chronic cyclodextrin treatment of murine Niemann-Pick C disease ameliorates neuronal cholesterol and glycosphingolipid storage and disease progression, PLoS One, 4 (2009) e6951. https://doi.org/10.1371/journal.pone.0006951

[11] C.H. Vite, J.H. Bagel, G.P. Swain, M. Prociuk, T.U. Sikora, V.M. Stein, P. O'Donnell, T. Ruane, S. Ward, A. Crooks, S. Li, E. Mauldin, S. Stellar, M. De Meulder, M.L. Kao, D.S. Ory, C. Davidson, M.T. Vanier, S.U. Walkley, Intracisternal cyclodextrin prevents cerebellar dysfunction and Purkinje cell death in feline Niemann-Pick type C1 disease, Sci Transl Med, 7 (2015) 276ra226. https://doi.org/10.1126/scitranslmed.3010101

[12] B. Liu, H. Li, J.J. Repa, S.D. Turley, J.M. Dietschy, Genetic variations and treatments that affect the lifespan of the NPC1 mouse, J Lipid Res, 49 (2008) 663-669. https://doi.org/M700525-JLR200 [pii] 10.1194/jlr.M700525-JLR200

[13] D.S. Ory, E.A. Ottinger, N.Y. Farhat, K.A. King, X. Jiang, L. Weissfeld, E. Berry-Kravis, C.D. Davidson, S. Bianconi, L.A. Keener, R. Rao, A. Soldatos, R. Sidhu, K.A. Walters, X. Xu, A. Thurm, B. Solomon, W.J. Pavan, B.N. Machielse, M. Kao, S.A. Silber, J.C. McKew, C.C. Brewer, C.H. Vite, S.U. Walkley, C.P. Austin, F.D. Porter, Intrathecal 2-hydroxypropyl-beta-cyclodextrin decreases neurological disease progression in Niemann-Pick disease, type C1: a non-randomised, open-label, phase 1-2 trial, Lancet, 390 (2017) 1758-1768. https://doi.org/10.1016/S0140-6736(17)31465-4

[14] A. Aqul, B. Liu, C.M. Ramirez, A.A. Pieper, S.J. Estill, D.K. Burns, B. Liu, J.J. Repa, S.D. Turley, J.M. Dietschy, Unesterified cholesterol accumulation in late endosomes/lysosomes causes neurodegeneration and is prevented by driving cholesterol export from this compartment, J Neurosci, 31 (2011) 9404-9413. https://doi.org/10.1523/JNEUROSCI.1317-11.2011

[15] C.C. Pontikis, C.D. Davidson, S.U. Walkley, F.M. Platt, D.J. Begley, Cyclodextrin alleviates neuronal storage of cholesterol in Niemann-Pick C disease without evidence of detectable blood-brain barrier permeability, J Inherit Metab Dis, 36 (2013) 491-498. https://doi.org/10.1007/s10545-012-9583-x

[16] B. Tortelli, H. Fujiwara, J.H. Bagel, J. Zhang, R. Sidhu, X. Jiang, N.M. Yanjanin, R.K. Shankar, N. Carillo-Carasco, J. Heiss, E. Ottinger, F.D. Porter, J.E. Schaffer, C.H. Vite, D.S. Ory, Cholesterol homeostatic responses provide biomarkers for monitoring treatment for the neurodegenerative disease Niemann-Pick C1 (NPC1), Hum Mol Genet, 23 (2014) 6022-6033. https://doi.org/10.1093/hmg/ddu331

[17] C. Yang, S. Rahimpour, J. Lu, K. Pacak, B. Ikejiri, R.O. Brady, Z. Zhuang, Histone deacetylase inhibitors increase glucocerebrosidase activity in Gaucher disease by modulation of molecular chaperones, Proc Natl Acad Sci U S A, 110 (2013) 966-971. https://doi.org/10.1073/pnas.1221046110

[18] K.J. Falkenberg, R.W. Johnstone, Histone deacetylases and their inhibitors in cancer, neurological diseases and immune disorders, Nat Rev Drug Discov, 13 (2014) 673-691. https://doi.org/10.1038/nrd4360

[19] A.B. Munkacsi, F.W. Chen, M.A. Brinkman, K. Higaki, G.D. Gutierrez, J. Chaudhari, J.V. Layer, A. Tong, M. Bard, C. Boone, Y.A. Ioannou, S.L. Sturley, An "exacerbate-reverse" strategy in yeast identifies histone deacetylase inhibition as a correction for cholesterol and sphingolipid transport defects in human Niemann-Pick type C disease, J Biol Chem, 286 (2011) 23842-23851. https://doi.org/10.1074/jbc.M111.227645

[20] N.H. Pipalia, C.C. Cosner, A. Huang, A. Chatterjee, P. Bourbon, N. Farley, P. Helquist, O. Wiest, F.R. Maxfield, Histone deacetylase inhibitor treatment dramatically reduces cholesterol accumulation in Niemann-Pick type C1 mutant human fibroblasts, Proc Natl Acad Sci U S A, 108 (2011) 5620-5625.

[21] N.H. Pipalia, K. Subramanian, S. Mao, H. Ralph, D.M. Hutt, S.M. Scott, W.E. Balch, F.R. Maxfield, Histone deacetylase inhibitors correct the cholesterol storage defect in most Niemann-Pick C1 mutant cells, J Lipid Res, 58 (2017) 695-708. https://doi.org/10.1194/jlr.M072140

[22] M. Praggastis, B. Tortelli, J. Zhang, H. Fujiwara, R. Sidhu, A. Chacko, Z. Chen, C. Chung, A.P. Lieberman, J. Sikora, C. Davidson, S.U. Walkley, N.H. Pipalia, F.R. Maxfield, J.E. Schaffer, D.S. Ory, A murine Niemann-Pick C1 I1061T knock-in model recapitulates the pathological features of the most prevalent human disease allele, J Neurosci, 35 (2015) 8091-8106. https://doi.org/10.1523/JNEUROSCI.4173-14.2015

[23] Phase 1/2 Study of Vorinostat Therapy in Niemann-Pick Disease, Type C1.

[24] A.B. Munkacsi, N. Hammond, R.T. Schneider, D.S. Senanayake, K. Higaki, K. Lagutin, S.J. Bloor, D.S. Ory, R.A. Maue, F.W. Chen, A. Hernandez-Ono, N. Dahlson, J.J. Repa, H.N. Ginsberg, Y.A. Ioannou, S.L. Sturley, Normalization of Hepatic Homeostasis in the Npc1(nmf164) Mouse Model of Niemann-Pick Type C Disease Treated with the Histone Deacetylase Inhibitor Vorinostat, J Biol Chem, 292 (2017) 4395-4410. https://doi.org/10.1074/jbc.M116.770578

[25] J.E. Hanson, H. La, E. Plise, Y.H. Chen, X. Ding, T. Hanania, E.V. Sabath, V. Alexandrov, D. Brunner, E. Leahy, P. Steiner, L. Liu, K. Scearce-Levie, Q. Zhou, SAHA enhances synaptic function and plasticity in vitro but has limited brain availability in vivo and does not impact cognition, PLoS One, 8 (2013) e69964. https://doi.org/10.1371/journal.pone.0069964

[26] M.S. Alam, M. Getz, K. Haldar, Chronic administration of an HDAC inhibitor treats both neurological and systemic Niemann-Pick type C disease in a mouse model, Sci Transl Med, 8 (2016) 326ra323. https://doi.org/10.1126/scitranslmed.aad9407

[27] M.S. Alam, B. Cooper, J.D. Farris, K. Haldar, Tolerance of chronic HDACi treatment for neurological, visceral and lung Niemann-Pick Type C disease in mice, Sci Rep, 8 (2018) 3875. https://doi.org/10.1038/s41598-018-22162-7

[28] S.K. Loftus, J.A. Morris, E.D. Carstea, J.Z. Gu, C. Cummings, A. Brown, J. Ellison, K. Ohno, M.A. Rosenfeld, D.A. Tagle, P.G. Pentchev, W.J. Pavan, Murine model of Niemann-Pick C disease: mutation in a cholesterol homeostasis gene, Science, 277 (1997) 232-235.

[29] P.G. Pentchev, A.E. Gal, A.D. Boothe, J. Fouks, F. Omodeo-Sale, R.O. Brady, A lysosomal storage disorder in mice characterized by the accumulation of several sphingolipids, Birth Defects Orig Artic Ser, 16 (1980) 225-230.

[30] J.C. Stowell, R.I. Huot, L. Van Voast, The synthesis of N-hydroxy-N'-phenyloctanediamide and its inhibitory effect on proliferation of AXC rat prostate cancer cells, J Med Chem, 38 (1995) 1411-1413.

[31] H. Jiang, R. Sidhu, H. Fujiwara, M. De Meulder, R. de Vries, Y. Gong, M. Kao, F.D. Porter, N.M. Yanjanin, N. Carillo-Carasco, X. Xu, E. Ottinger, M. Woolery, D.S. Ory, X. Jiang, Development and validation of sensitive LC-MS/MS assays for quantification of HP-beta-CD in human plasma and CSF, J Lipid Res, 55 (2014) 1537-1548. https://doi.org/10.1194/jlr.D050278

[32] E.E. Millard, K. Srivastava, L.M. Traub, J.E. Schaffer, D.S. Ory, Niemann-pick type C1 (NPC1) overexpression alters cellular cholesterol homeostasis, J Biol Chem, 275 (2000) 38445-38451. https://doi.org/10.1074/jbc.M003180200

[33] A. Schweizer, J. Rohrer, J.W. Slot, H.J. Geuze, S. Kornfeld, Reassessment of the subcellular localization of p63, J Cell Sci, 108 (Pt 6) (1995) 2477-2485.

[34] M. Fan, R. Sidhu, H. Fujiwara, B. Tortelli, J. Zhang, C. Davidson, S.U. Walkley, J.H. Bagel, C. Vite, N.M. Yanjanin, F.D. Porter, J.E. Schaffer, D.S. Ory, Identification of Niemann-Pick C1 disease biomarkers through sphingolipid profiling, J Lipid Res, 54 (2013) 2800-2814. https://doi.org/10.1194/jlr.M040618

[35] S. Zhou, C. Davidson, R. McGlynn, G. Stephney, K. Dobrenis, M.T. Vanier, S.U. Walkley, Endosomal/lysosomal processing of gangliosides affects neuronal cholesterol sequestration in Niemann-Pick disease type C, Am J Pathol, 179 (2011) 890-902. https://doi.org/10.1016/j.ajpath.2011.04.017

[36] L. Riva, S.M. Blaney, R. Dauser, J.G. Nuchtern, J. Durfee, L. McGuffey, S.L. Berg, Pharmacokinetics and cerebrospinal fluid penetration of CI-994 (N-acetyldinaline) in the nonhuman primate, Clinical Cancer Research, 6 (2000) 994-997.

[37] C.D. Davidson, Y.I. Fishman, I. Puskas, J. Szeman, T. Sohajda, L.A. McCauliff, J. Sikora, J. Storch, M.T. Vanier, L. Szente, S.U. Walkley, K. Dobrenis, Efficacy and ototoxicity of different cyclodextrins in Niemann-Pick C disease, Ann Clin Transl Neurol, 3 (2016) 366-380. https://doi.org/10.1002/acn3.306

[38] W.S. Xu, R.B. Parmigiani, P.A. Marks, Histone deacetylase inhibitors: molecular mechanisms of action, Oncogene, 26 (2007) 5541-5552. https://doi.org/10.1038/sj.onc.1210620

[39] T. Kirkegaard, J. Gray, D.A. Priestman, K.L. Wallom, J. Atkins, O.D. Olsen, A. Klein, S. Drndarski, N.H. Petersen, L. Ingemann, D.A. Smith, L. Morris, C. Bornaes, S.H. Jorgensen, I. Williams, A. Hinsby, C. Arenz, D. Begley, M. Jaattela, F.M. Platt, Heat shock protein-based therapy as a potential candidate for treating the sphingolipidoses, Sci Transl Med, 8 (2016) 355ra118. https://doi.org/10.1126/scitranslmed.aad9823

[40] H. Arima, K. Yunomae, T. Morikawa, F. Hirayama, K. Uekama, Contribution of cholesterol and phospholipids to inhibitory effect of dimethyl-beta-cyclodextrin on efflux function of P-glycoprotein and multidrug resistance-associated protein 2 in vinblastine-resistant Caco-2 cell monolayers, Pharm Res, 21 (2004) 625-634.

[41] M.J. Kruhlak, M.J. Hendzel, W. Fischle, N.R. Bertos, S. Hameed, X.J. Yang, E. Verdin, D.P. Bazett-Jones, Regulation of global acetylation in mitosis through loss of histone acetyltransferases and deacetylases from chromatin, J Biol Chem, 276 (2001) 38307-38319. https://doi.org/10.1074/jbc.M100290200

Highlights

- *In vivo* efficacy of HDAC inhibitor formulation due to enhanced cyclodextrin PK
- HDAC inhibitors are ineffective in ameliorating neurovisceral disease in *Npc1* mice
- Lack of efficacy in non-dividing cells may explain HDAC inhibitor failure in vivo

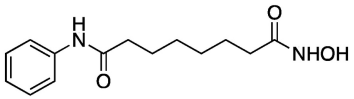

Suberoylanilide Hydroxamic Acid
(vorinostat)

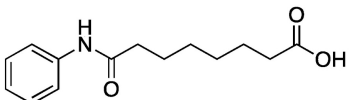

Suberoylanilide Acid
(inactive vorinostat analog, IVA)

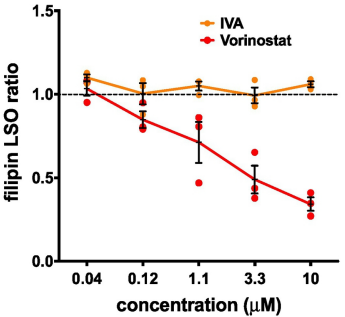

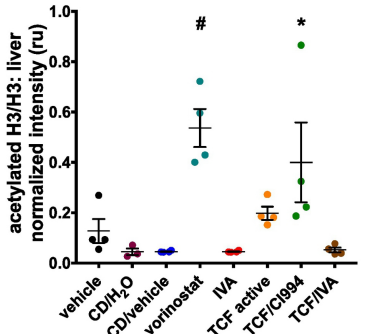

Figure 1

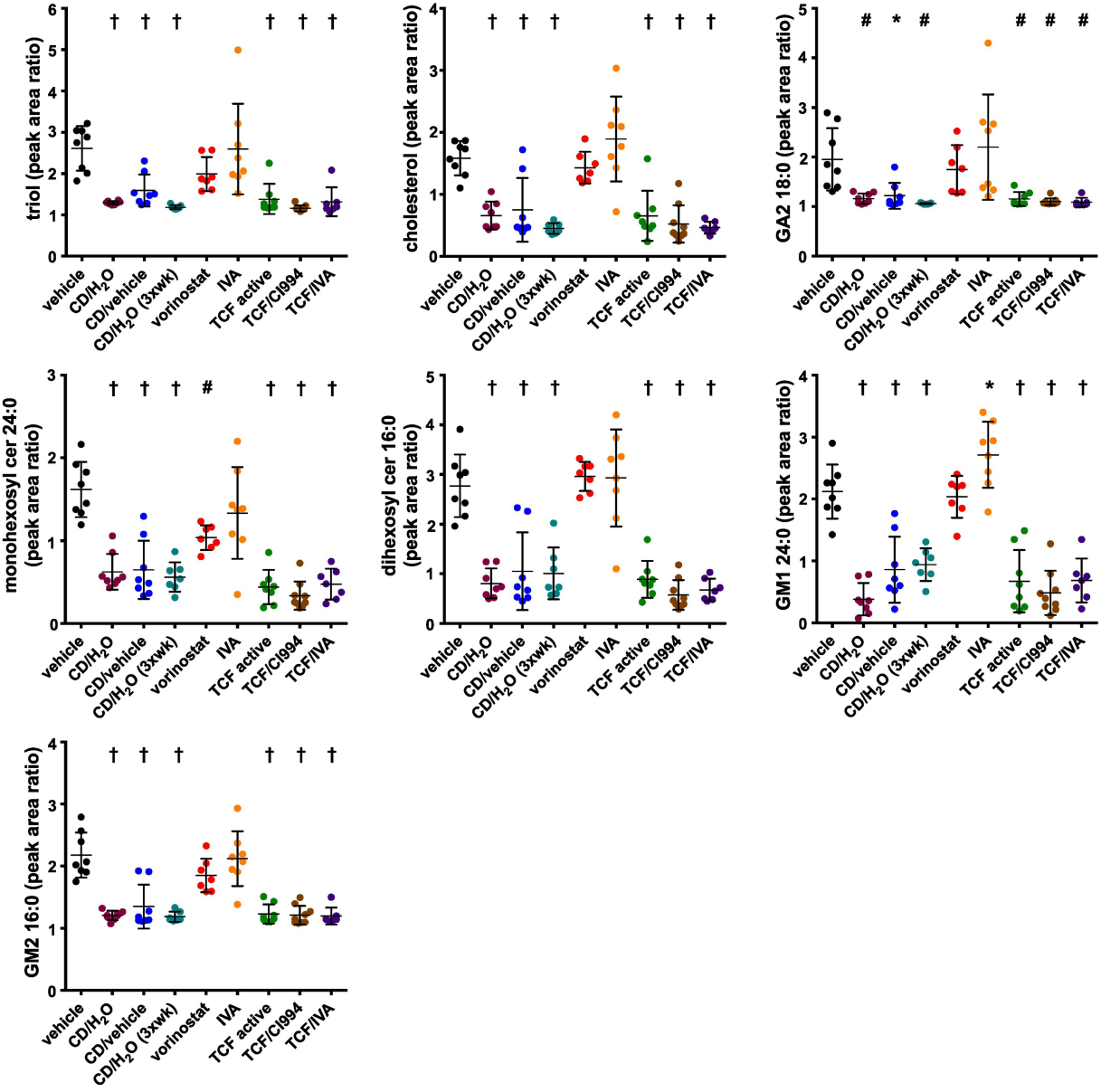
triol (peak area ratio)
cholesterol (peak area ratio)
GA2 18:0 (peak area ratio)
monohexosyl cer 24:0 (peak area ratio)
dihexosyl cer 16:0 (peak area ratio)
GM1 24:0 (peak area ratio)
GM2 16:0 (peak area ratio)
vehicle
CD/H2O
CD/vehicle
CD/H2O (3xwk)
vorinostat
IVA
TCF active
TCF/CI994
TCF/IVA

Figure 2

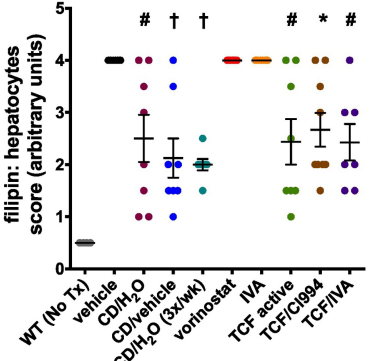
filipin: hepatocytes score (arbitrary units)
5
4
3
2
1
0
† †
*
WT (No Tx)
vehicle
CD/H2O
CD/vehicle
CD/H2O (3x/wk)
vorinostat
IVA
TCF active
TCF/CI994
TCF/IVA

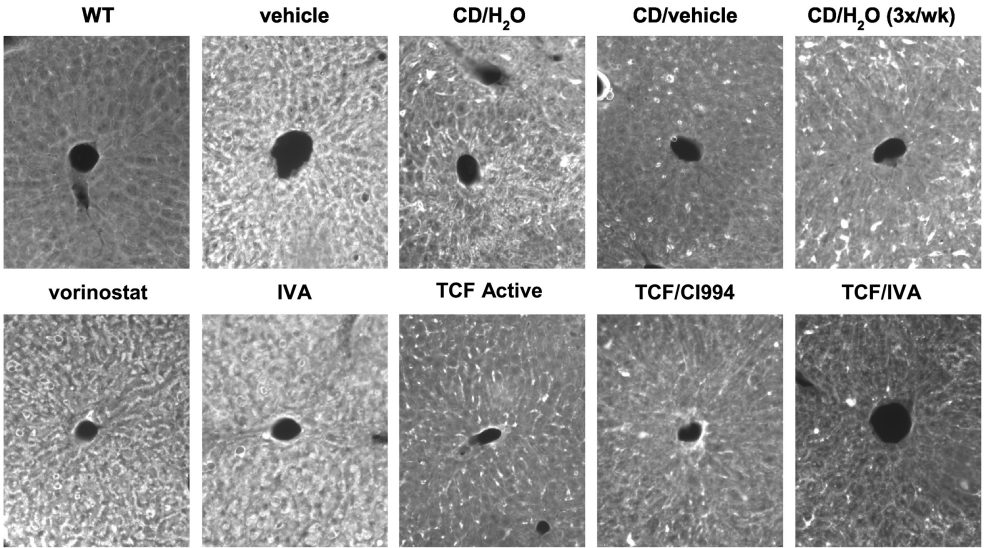
WT
vehicle
CD/H2O
CD/vehicle
CD/H2O (3x/wk)
vorinostat
IVA
TCF Active
TCF/CI994
TCF/IVA

Figure 3

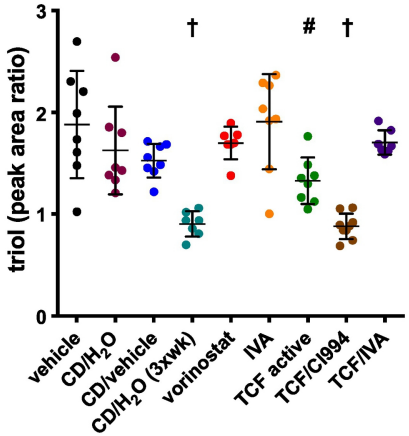
triol (peak area ratio)
†
#
†
vehicle
CD/H2O
CD/vehicle
CD/H2O (3xwk)
vorinostat
IVA
TCF active
TCF/CI994
TCF/IVA

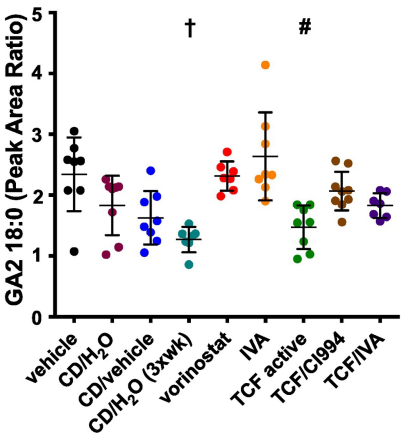
GA2 18:0 (Peak Area Ratio)
†
#
vehicle
CD/H2O
CD/vehicle
CD/H2O (3xwk)
vorinostat
IVA
TCF active
TCF/CI994
TCF/IVA

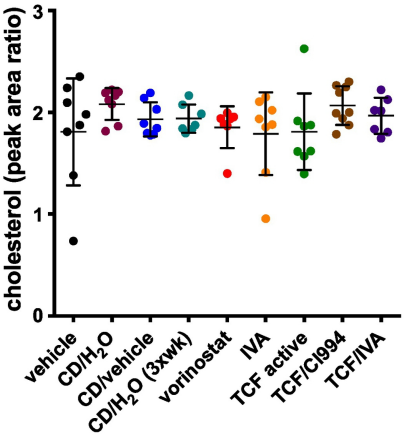
cholesterol (peak area ratio)
vehicle
CD/H2O
CD/vehicle
CD/H2O (3xwk)
vorinostat
IVA
TCF active
TCF/CI994
TCF/IVA

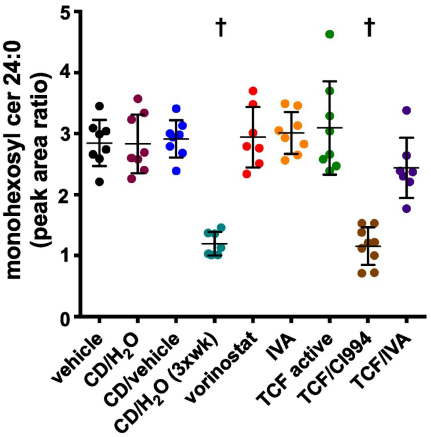
monohexosyl cer 24:0 (peak area ratio)
†
†
vehicle
CD/H2O
CD/vehicle
CD/H2O (3xwk)
vorinostat
IVA
TCF active
TCF/CI994
TCF/IVA

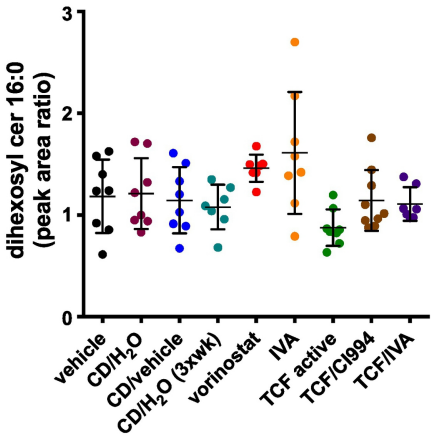
dihexosyl cer 16:0 (peak area ratio)
vehicle
CD/H2O
CD/vehicle
CD/H2O (3xwk)
vorinostat
IVA
TCF active
TCF/CI994
TCF/IVA

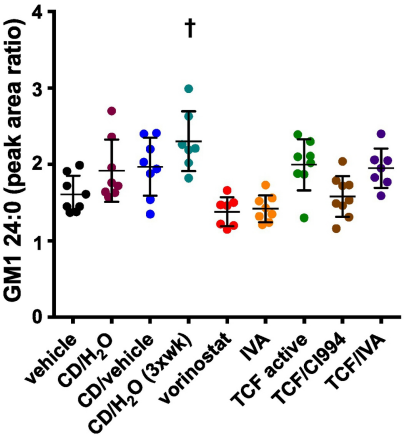
GM1 24:0 (peak area ratio)
†
vehicle
CD/H2O
CD/vehicle
CD/H2O (3xwk)
vorinostat
IVA
TCF active
TCF/CI994
TCF/IVA

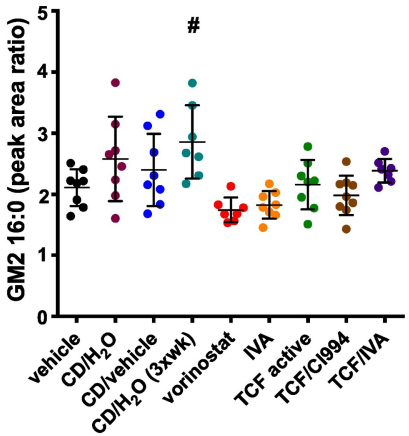
GM2 16:0 (peak area ratio)
#
vehicle
CD/H2O
CD/vehicle
CD/H2O (3xwk)
vorinostat
IVA
TCF active
TCF/CI994
TCF/IVA

Figure 4

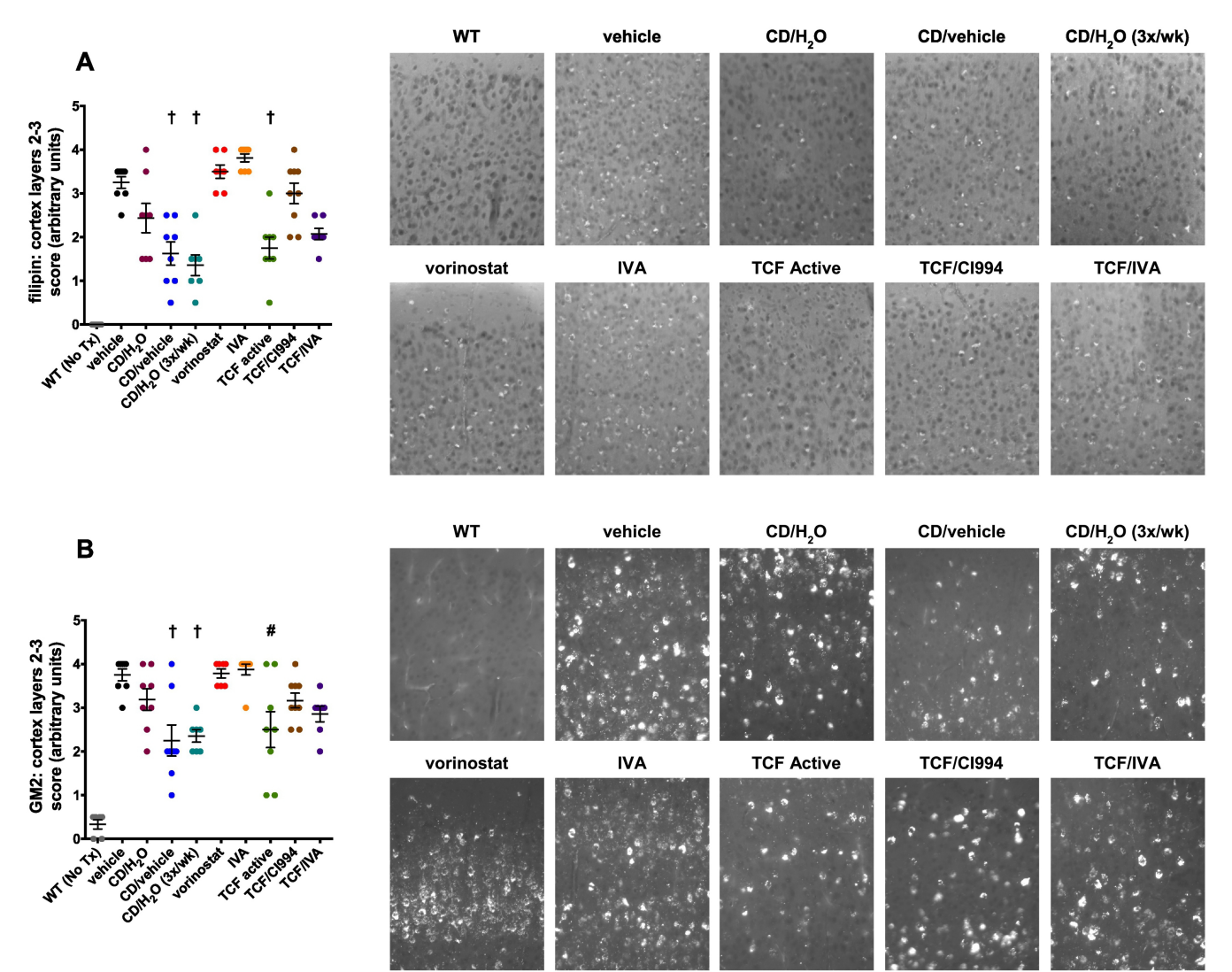
A
filipin: cortex layers 2-3 score (arbitrary units)
0
1
2
3
4
5
†
†
†
WT (No Tx)
vehicle
CD/H2O
CD/vehicle
CD/H2O (3x/wk)
vorinostat
IVA
TCF active
TCF/CI994
TCF/IVA
WT
vehicle
CD/H2O
CD/vehicle
CD/H2O (3x/wk)
vorinostat
IVA
TCF Active
TCF/CI994
TCF/IVA
B
GM2: cortex layers 2-3 score (arbitrary units)
0
1
2
3
4
5
†
†
#
WT (No Tx)
vehicle
CD/H2O
CD/vehicle
CD/H2O (3x/wk)
vorinostat
IVA
TCF active
TCF/CI994
TCF/IVA
WT
vehicle
CD/H2O
CD/vehicle
CD/H2O (3x/wk)
vorinostat
IVA
TCF Active
TCF/CI994
TCF/IVA

Figure 5

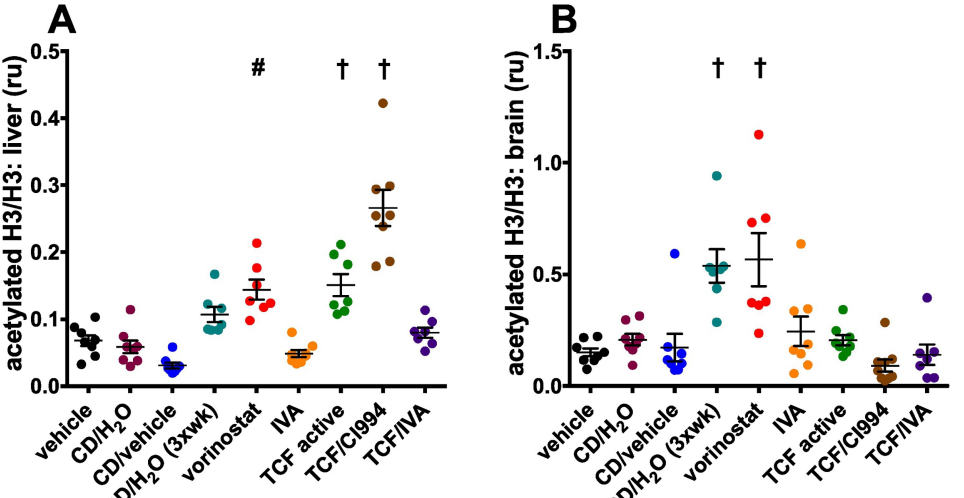
A
acetylated H3/H3: liver (ru)
0.5
0.4
0.3
0.2
0.1
0.0
#
†
†
vehicle
CD/H2O
CD/vehicle
CD/H2O (3xwk)
vorinostat
IVA
TCF active
TCF/Cl994
TCF/IVA
B
acetylated H3/H3: brain (ru)
1.5
1.0
0.5
0.0
†
†
vehicle
CD/H2O
CD/vehicle
CD/H2O (3xwk)
vorinostat
IVA
TCF active
TCF/Cl994
TCF/IVA

Figure 6

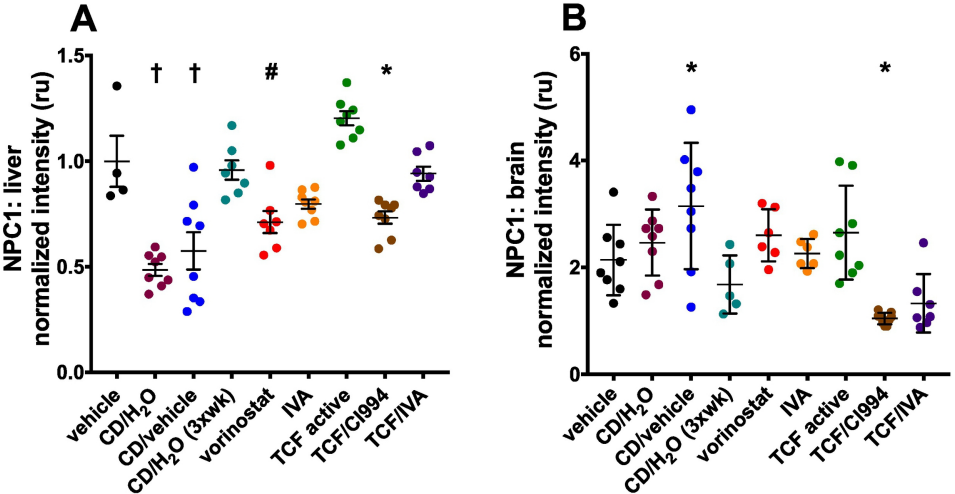
A
NPC1: liver
normalized intensity (ru)
1.5
1.0
0.5
0.0
†
†
#
*
vehicle
CD/H2O
CD/vehicle
CD/H2O (3xwk)
vorinostat
IVA
TCF active
TCF/CI994
TCF/IVA
B
NPC1: brain
normalized intensity (ru)
6
4
2
0
*
*
vehicle
CD/H2O
CD/vehicle
CD/H2O (3xwk)
vorinostat
IVA
TCF active
TCF/CI994
TCF/IVA

Figure 7

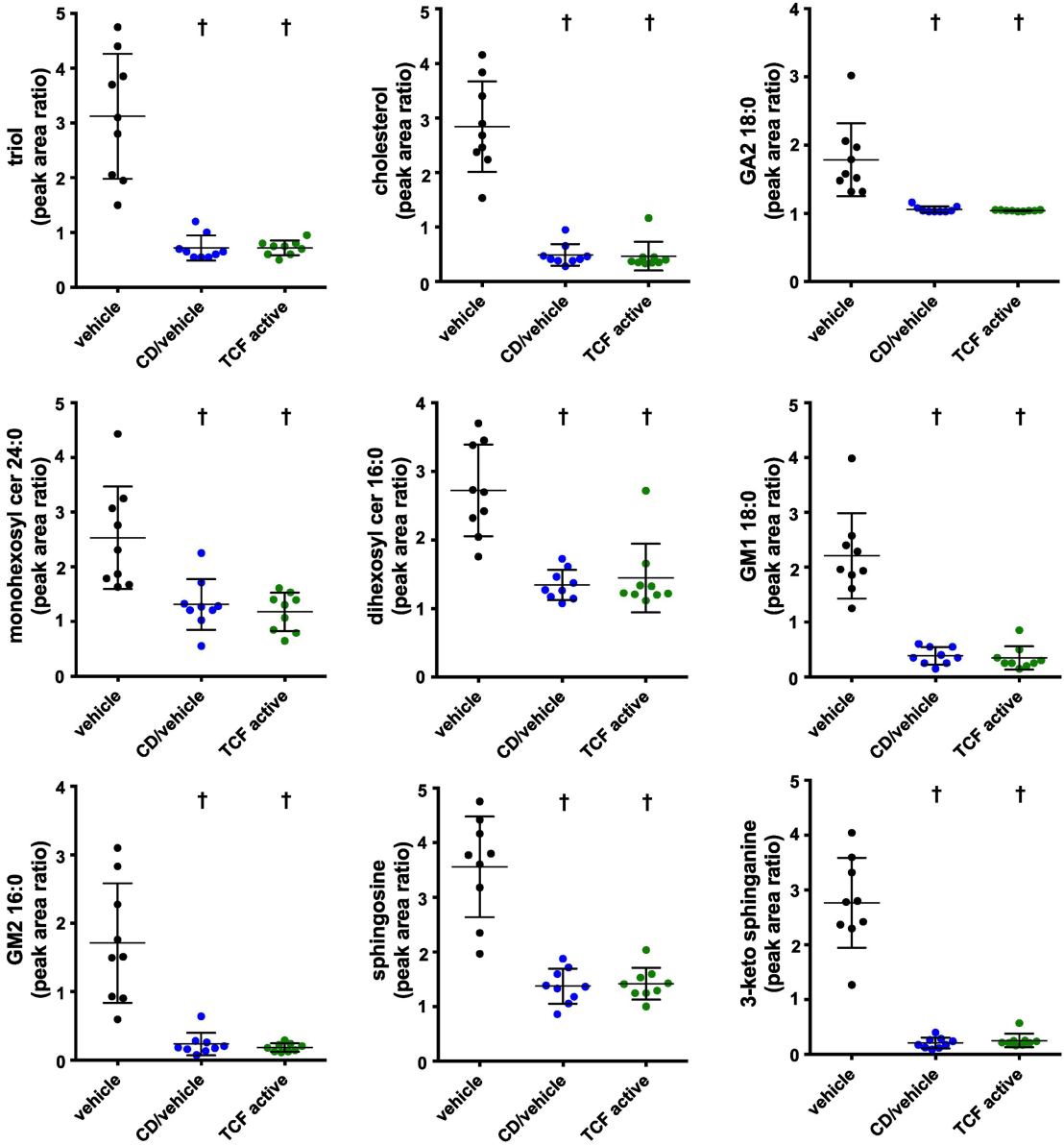
triol (peak area ratio)
cholesterol (peak area ratio)
GA2 18:0 (peak area ratio)
monohexosyl cer 24:0 (peak area ratio)
dihexosyl cer 16:0 (peak area ratio)
GM1 18:0 (peak area ratio)
GM2 16:0 (peak area ratio)
sphingosine (peak area ratio)
3-keto sphinganine (peak area ratio)
†
vehicle
CD/vehicle
TCF active

Figure 8

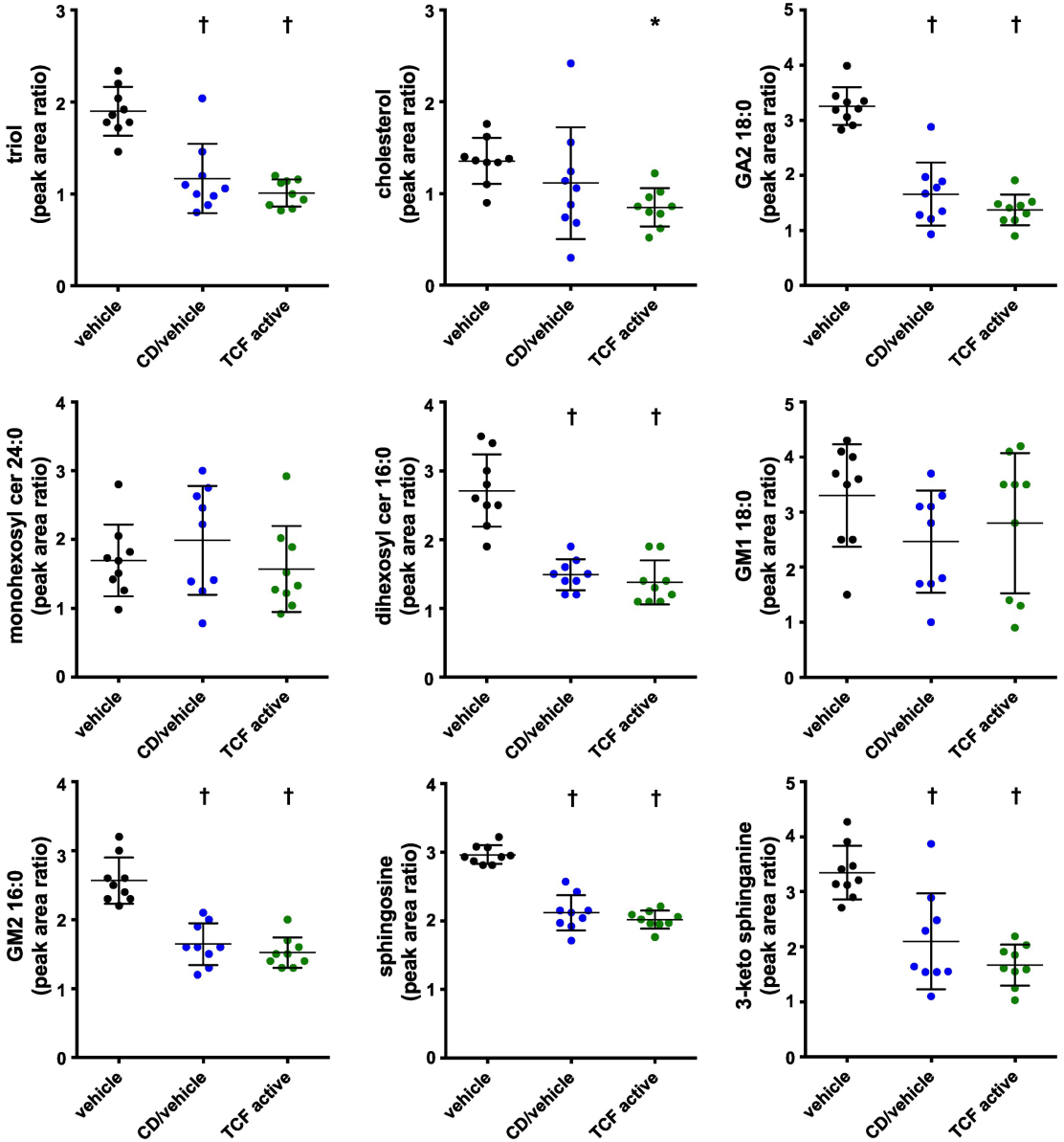
triol (peak area ratio)
cholesterol (peak area ratio)
GA2 18:0 (peak area ratio)
monohexosyl cer 24:0 (peak area ratio)
dihexosyl cer 16:0 (peak area ratio)
GM1 18:0 (peak area ratio)
GM2 16:0 (peak area ratio)
sphingosine (peak area ratio)
3-keto sphinganine (peak area ratio)
vehicle
CD/vehicle
TCF active
†
*

Figure 9

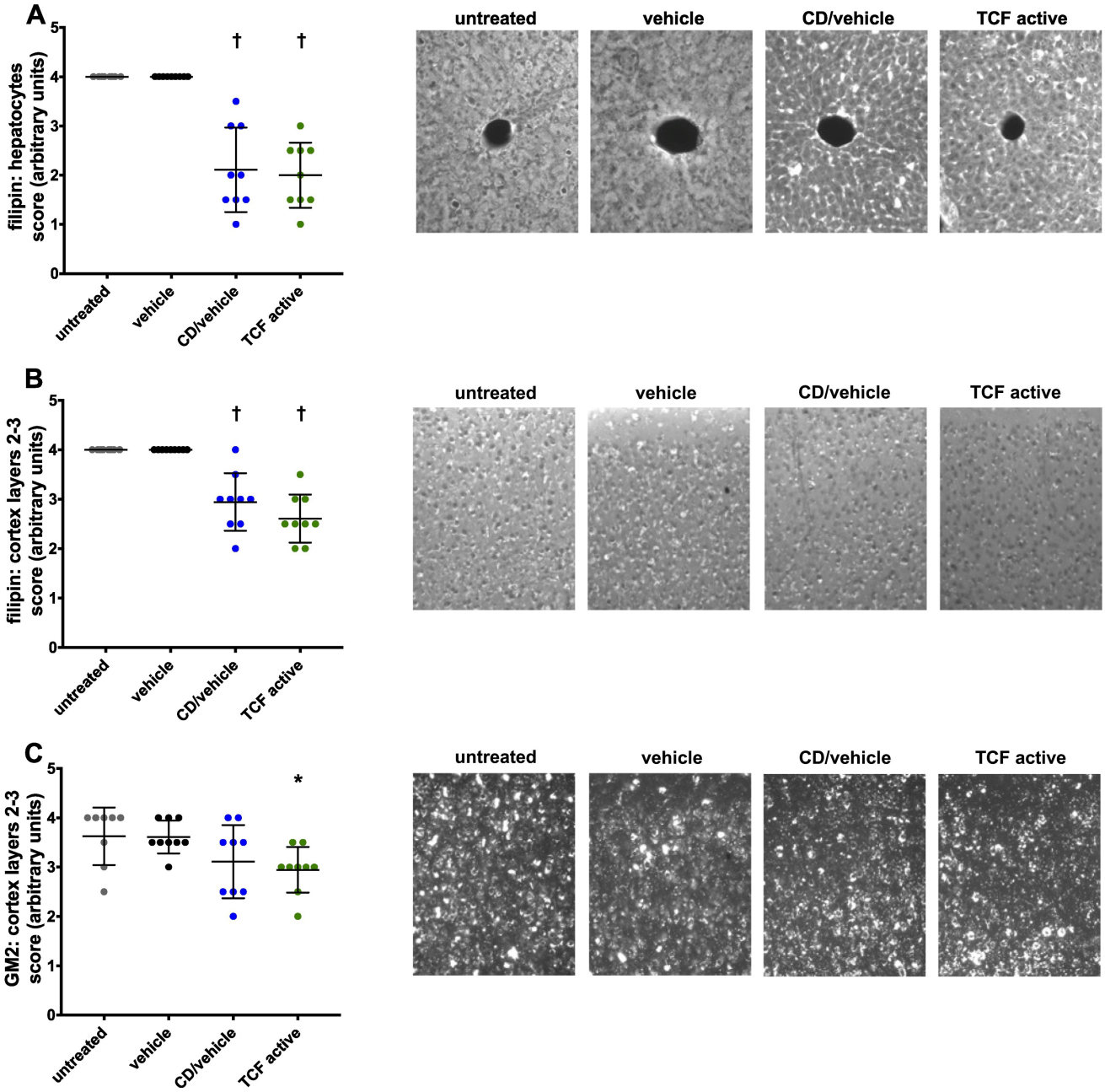
A
filipin: hepatocytes score (arbitrary units)
0
1
2
3
4
5
†
†
untreated
vehicle
CD/vehicle
TCF active
untreated
vehicle
CD/vehicle
TCF active
B
filipin: cortex layers 2-3 score (arbitrary units)
0
1
2
3
4
5
†
†
untreated
vehicle
CD/vehicle
TCF active
untreated
vehicle
CD/vehicle
TCF active
C
GM2: cortex layers 2-3 score (arbitrary units)
0
1
2
3
4
5
*
untreated
vehicle
CD/vehicle
TCF active
untreated
vehicle
CD/vehicle
TCF active

Figure 10

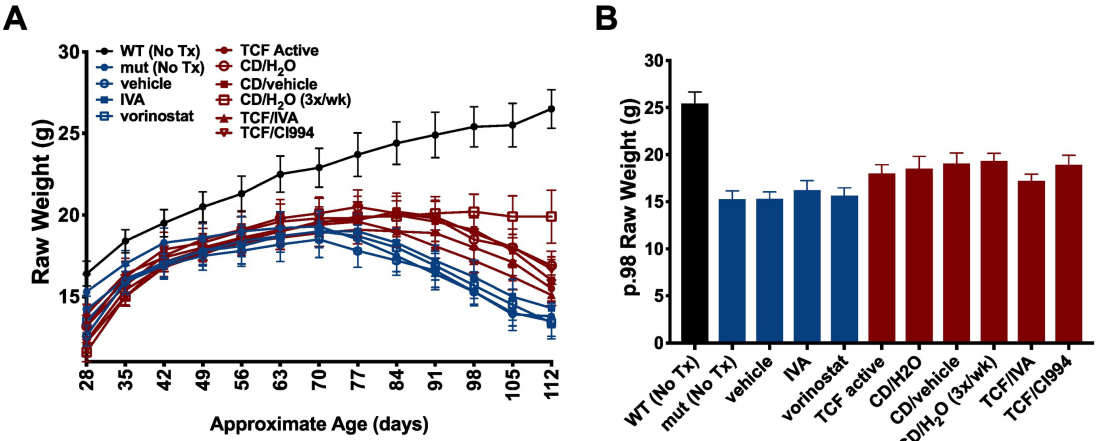
A
WT (No Tx)
mut (No Tx)
vehicle
IVA
vorinostat
TCF Active
CD/H2O
CD/vehicle
CD/H2O (3x/wk)
TCF/IVA
TCF/CI994
Raw Weight (g)
30
25
20
15
28
35
42
49
56
63
70
77
84
91
98
105
112
Approximate Age (days)
B
p.98 Raw Weight (g)
30
25
20
15
10
5
0
WT (No Tx)
mut (No Tx)
vehicle
IVA
vorinostat
TCF active
CD/H2O
CD/vehicle
CD/H2O (3x/wk)
TCF/IVA
TCF/CI994

Figure 11

A

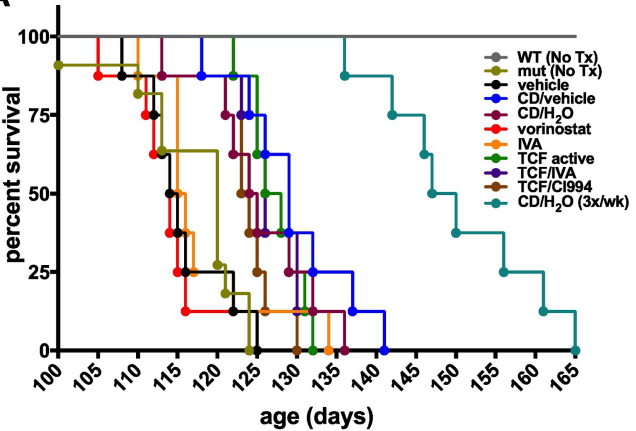

B

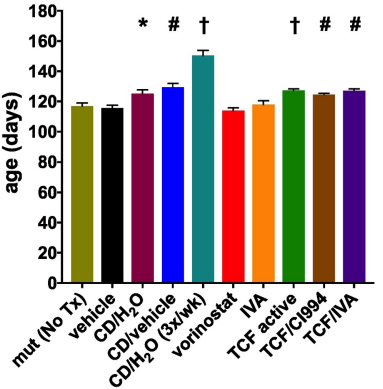

C

Treatment Group	Mean Lifespan (days)	Median Lifespan (days)
WT	342.6	364.0
Mutant	116.8	120.0
vehicle	115.6	114.5
CD/H_2O	125.2	124.5
CD/vehicle	129.5	129.0
CD/H_2O (3x/wk)	150.4	148.5
vorinostat	113.8	114.0
IVA	118.0	115.5
TCF active	127.2	127.0
TCF/CI994	124.5	123.5
TCF/IVA	127.0	126.0

Figure 12

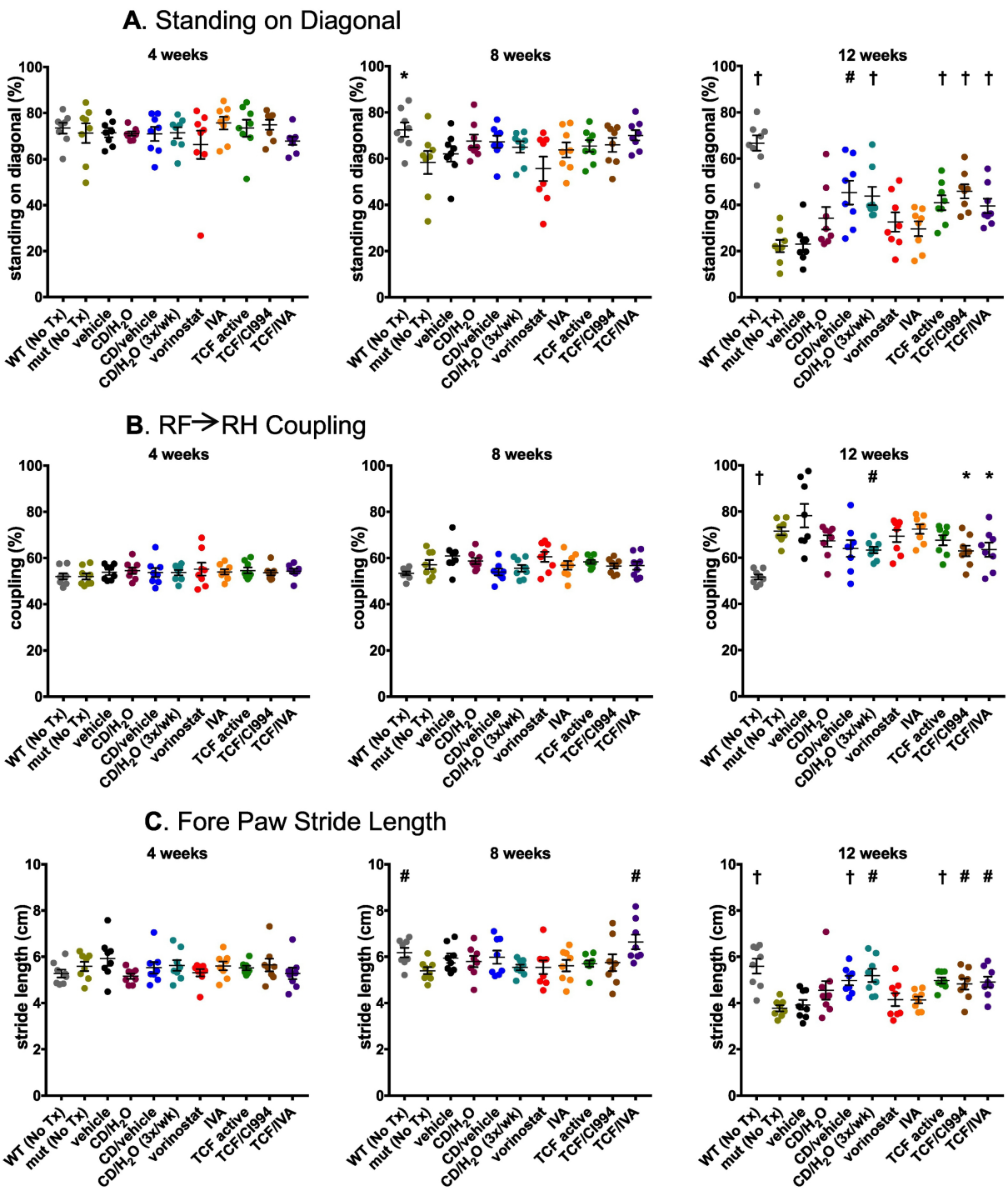
A. Standing on Diagonal
4 weeks
8 weeks
12 weeks
standing on diagonal (%)
B. RF→RH Coupling
coupling (%)
C. Fore Paw Stride Length
stride length (cm)
WT (No Tx)
mut (No Tx)
vehicle
CD/H2O
CD/vehicle
CD/H2O (3x/wk)
vorinostat
IVA
TCF active
TCF/CI994
TCF/IVA

Figure 13

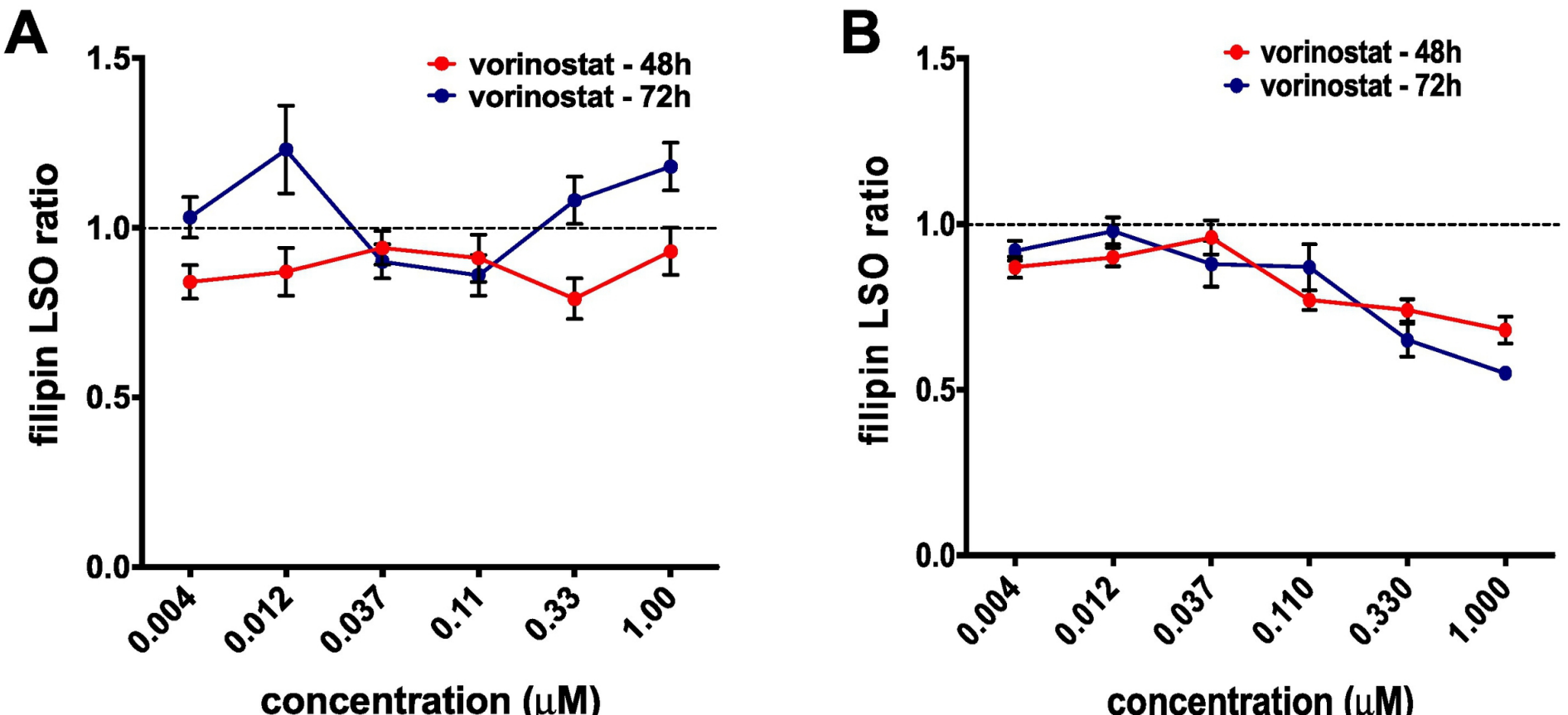
A
B
vorinostat - 48h
vorinostat - 72h
filipin LSO ratio
1.5
1.0
0.5
0.0
0.004
0.012
0.037
0.11
0.33
1.00
0.110
0.330
1.000
concentration (μM)

Figure 14